

# Medical Imaging Generated Dynamic Prosthetic Sockets

---

**FINAL REPORT**

**CNTS 2008-00059**

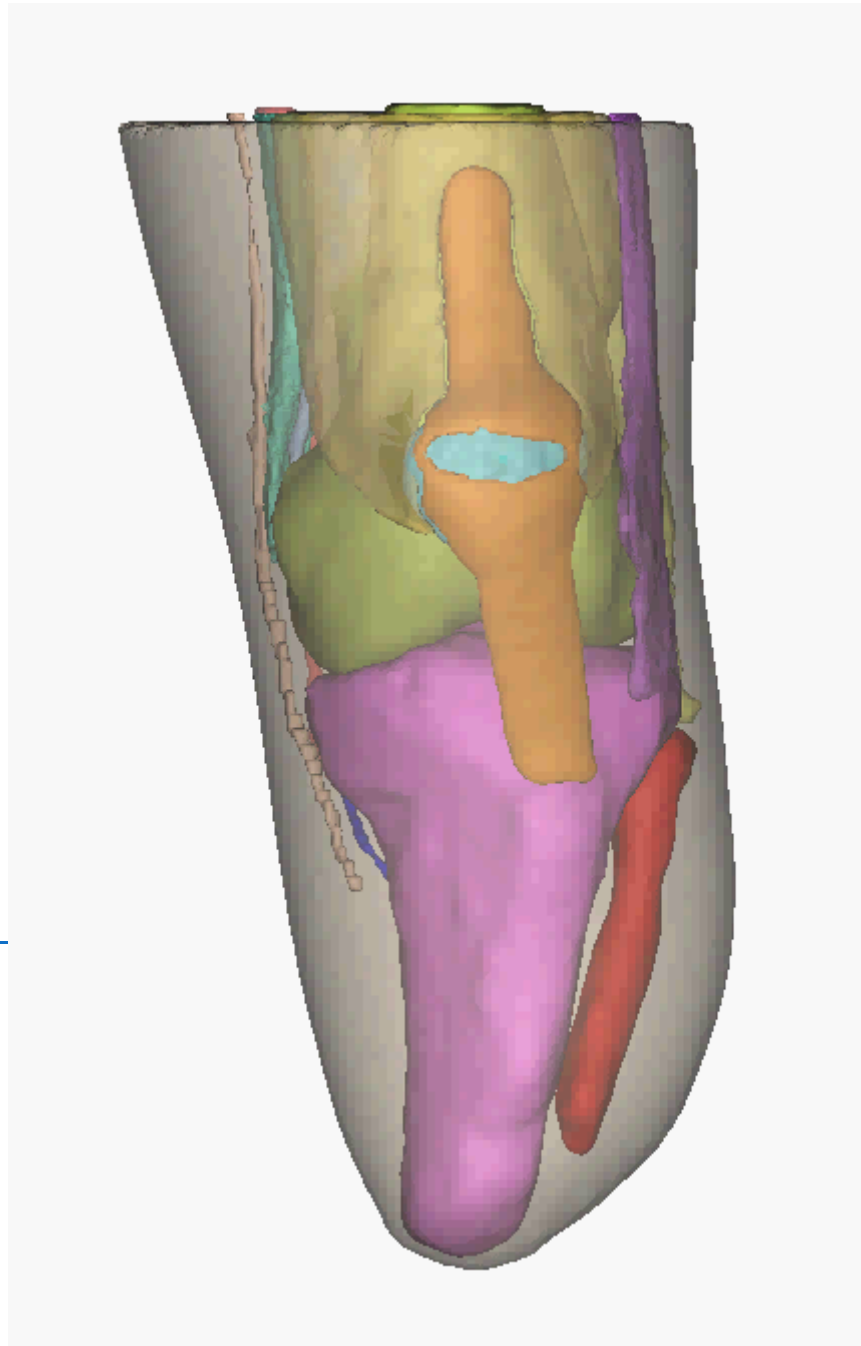
**May 31, 2011**

**Robert S. Kistenberg, PI**

**Shayne Kondor, Co-PI**

**Samer Tawfik, PhD, Co-Investigator**

**Michael Terk, M.D., Co-Investigator**



**Georgia Institute  
of Technology**



## Acknowledgements

This Project was sponsored by the Office of Naval Research through the South Carolina Research Authorities' Prosthetic Orthotic Manufacturing Initiative. Special recognition is also given to Dr. Chris Norfolk for his support and guidance through this project.



## **Executive Summary**

The Medical Imaging Generate Dynamic Prosthetic Socket project was an ambitious 2 year effort which aimed to develop a system that would allow for direct MRI scanning of residual limbs to generate prosthetic sockets that were based upon the underlying anatomical structures whilst assessing the pressures these sockets would impose upon the residual limbs through finite element analysis.

The process was divided up into specific tasks including the Non-Deformational Shell, MRI Scanning, Segmenting and Modeling the Residual Limb, Fabrication of the Prosthetic Socket, Finite Element Analysis and Socket Iterations. Completion of the final tasks was entirely dependent on completion of the earlier tasks.

Processes were established and tested for the Non-Deformation Shell, MRI Scanning, Segmenting and Modeling the Residual Limb, Fabrication of the Prosthetic Socket and Finite Element Analysis. Validation of the finite element analysis required that the assumptions made for pressure in the socket be tested and confirmed. This step proved to be the most challenging due to the absence of an accurate and consistent pressure measurement system. Because we were ultimately unable to obtain in-socket pressure measurement data, the socket iteration task was not completed.

This project, however, was successful in a number of ways. The fabrication method of the non-deformational shell was completed and tested. Many protocols for RL scanning were investigated and settings were optimized for obtaining scans for both transtibial amputations and transfemoral amputations which then facilitated residual limb segmentation. The process for segmentation proved to be cumbersome and difficult to achieve without significant experience on the part of the person performing this task. Automated segmentation is still not developed to the point where this process is feasible in clinical practice.

Once the arduous process of segmentation was completed, the residual limb modeling allowed for the prosthetist to “look into” a residual limb for the first time ever. This allowed for precise modifications of the anatomical structures but emphasized how little we know about how to load and relieve these anatomical structures. The process

of transferring the residual limb data between multiple software programs (MIMICS, 3-MATIC, ABAQUS & CANFIT) was cumbersome and required creative work around solutions in order to maintain data fidelity while allowing the job of each software program to be completed.

Once the rectified model was completed, the answer to how the anatomical structures could be loaded and relieved was to be solved by the finite element modeling (FEA). The FEA process also required an extensive amount of time and expertise on the part of the research however in the end; the process was established and refined, resulting in a straight forward method to perform FEA on sockets including donning, static standing and single limb support. We were not able to establish the ability to generate residual limb pressures and stresses in a dynamic state.

It was at this point that the project stalled. We made multiple attempts to obtain valid and reliable socket pressure measurements in order to validate the FEA assumptions. While each of the three transtibial and three transfemoral subjects' sockets were being moved through the process concurrently, the process needed to be completed for the first of each subject type to its conclusion before we progressed with the other two of each subject type. The lessons learned from the first transtibial and first transfemoral subject needed to be applied to the subsequent subjects so that process enhancements could be implemented.

In the end, the first transtibial subject, TT01, was fit with three iterations of sockets and then tested for socket pressure repeatedly over the course of the project however the pressure measurements, even with continued system refinements, proved inaccurate. Two iterations of each of the transtibial subjects were completed. Sockets were fabricated for the first and third transfemoral subjects and the first socket was fit to transfemoral subject TF01.

In summary, this project significantly enhanced our understanding about residual limb anatomy, the processes for obtaining residual anatomy through MRI scanning as well as the processes for performing finite element analysis on a residual limb/socket interface. It also identified a number of limitations that persist making automatic socket generation from MRI scanning impractical until these limitations are overcome.

# Table of Contents

Executive Summary .....	2
Table of Contents .....	4
Table of Figures .....	6
Table of Tables .....	7
Introduction .....	8
Background/Problem Statement .....	8
Objectives .....	9
Approach.....	10
Non-Deformation Shell .....	10
Fabrication of the non-deformational shell .....	10
MRI Scanning .....	13
Residual Limb Scanning Background .....	13
Overview of Scan Series.....	15
Trans-tibial Scanning Protocol .....	16
Trans-femoral Scanning Protocol.....	20
The IDEAL MRI Algorithm.....	21
Segmentation & Modeling.....	23
CAD Socket Design .....	32
Socket Design using 3matic.....	33
Socket Design using CANFIT – Transtibial Models.....	36
Socket Design using CANFIT – Transfemoral Models .....	39
FEA Analysis .....	41
FEA Introduction .....	41
FEA Model preparation .....	43
Model preparation, Individual anatomical entities .....	43
Model preparation, Interaction of anatomical entities .....	44
Model preparation, <i>CAD Link</i> export into STEP or IGES.....	49
FEA Process .....	51
Importing part (individual successive operations) .....	52
Meshing part (individual successive operations) .....	53
Property Module (Material assignment).....	56
Assembly Module .....	59
Step Module .....	60

Interaction Module .....	61
Load Module.....	63
Job Module.....	65
FEA Analysis Results.....	65
Analysis results, a transtibial case.....	65
<i>The pressure distribution</i> , identifying the major function of the gel liner .....	65
External versus internal load comparison, i.e. pressure versus stress .....	67
Analysis results, a transfemoral case .....	70
<i>The pressure distribution</i> , identifying the major function of the gel liner .....	70
<i>The stress distribution</i> , in the bones community.....	71
FEA Challenges .....	73
Pressure measurements and verification .....	73
Material models .....	73
<i>FEA prosthetist</i> .....	74
FEA Conclusions.....	74
Anatomically correct analysis .....	74
Alternative accurate load measurements .....	74
FEA Suggested future work .....	76
Results and Discussion.....	77
This project endeavored to meet the following aims: .....	77
Benefits Analysis (including final metrics tables) .....	79
Implementation Status.....	79
References.....	82

## Table of Figures

Figure 1: Anterior view of Subject TT1 in non-deformational shell .....	10
Figure 2: Lateral view of Subject TT1 in the non-deformational shell .....	10
Figure 3: Orientation of planes with representative scan for TT01 .....	15
Figure 5: Sagittal, Coronal and Axial view of Subject TT01 .....	16
Figure 4: GE Sigma HDxt 3.0T scanner .....	16
Figure 6: Mechanical Shift Artifact in TT subject .....	18
Figure 7: Chemical Shift Artifact in TT Subject .....	18
Figure 8: Example of a wrap artifact on a transfemoral subject scan .....	20
Figure 9: Example of TF01 Subject lying on his unaffected side with his legs strapped to assist with keeping them still .....	20
Figure 10: Example of TF01 subject lying on affected side for scan. This produced a wrap artifact.....	20
Figure 11: MIMICs user interface showing a TT residual limb.....	23
Figure 12: A- 3D geometry as obtained from MRI (left), B- Optimized smooth 3-D geometry (right).....	43
Figure 13: Overlapping boundaries of tissues (section above the knee in a trans-tibial case) .....	45
Figure 14: Overlaps between different tissue types .....	45
Figure 15: Modified surface of the Triceps muscle at the interface .....	47
Figure 16: Assembled bones, tendons and muscles (left leg – lateral and medial views) .....	48
Figure 17: The 3D geometry of fat tissue as obtained directly from segmentation .....	48
Figure 18: The final 3D geometry of fat tissue as obtained via Boolean operations.....	49
Figure 19: Analytical geometry of the muscle community as obtained from CAD Link..	50
Figure 20: 3-matic Logger feedback report providing the export process quality .....	50
Figure 21: Solid import options.....	52
Figure 22: Imported 3D solid analytical geometry of bones.....	53
Figure 23: Mesh module, seed part.....	54
Figure 24: Mesh module, mesh controls .....	55
Figure 25: Mesh module, element type .....	55
Figure 26: Mesh module, final mesh .....	56
Figure 27: The Mooney-Rivlin material model assigned to the muscle .....	57
Figure 28: A second order polynomial strain energy assigned to the fat .....	58
Figure 29: Exploded view of parts import .....	59
Figure 30: Identical global coordinate system for imported parts .....	59
Figure 31: Step Module .....	61
Figure 32: Extended contact matrix applied through ABAQUS detection tool .....	62
Figure 33: Socket interaction property with the gel liner.....	62
Figure 34: Boundary conditions applied to the RL.....	63
Figure 35: Predefined thermal field .....	64
Figure 36: Applied load for standing load case .....	64
Figure 37: Pressure comparison over gel liner vs. skin – anterior view.....	66
Figure 38: Pressure comparison over gel liner vs. skin – posterior view .....	66
Figure 39: Pressure comparison over gel liner vs. skin – lateral view .....	67
Figure 40: Pressure comparison over gel liner vs. skin – medial view .....	67

Figure 41: External vs. internal loads within the patellar tendon/bar .....	68
Figure 42: Undeformed shape vs. deformed shapes, associated to socket donning and dual limb support.....	69
Figure 43: Sectional view in the deformed shape at dual limb support.....	69
Figure 44: Pressure distribution over gel liner vs. skin – single limb support. Same pressure range or scale.....	70
Figure 45: Pressure distribution over gel liner vs. skin – single limb support. Different pressure range or scale.....	71
Figure 46: Stress distribution in the ischium.....	71
Figure 47: Stress distribution in the ischium with the socket in view .....	72
Figure 48: Sectional view for single limb support .....	72
Figure 49: Sample of one of the Zebra Sensor sockets fabricated for TT01 .....	73
Figure 50: Subject TT01 on Diagnostic socket instrumented with ZEBRA socket pressure sensors and with an IPECs unit distal to the socket .....	74
Figure 51: Standing exercise – force values .....	75
Figure 52: Standing exercise – moment values .....	76

## Table of Tables

Table 1: Fabrication of the non-deformational shell .....	12
Table 2: Examples of MRI scans of the Transtibial Subjects.....	19
Table 3: Representative scans of the TF 01 and TF 02 subjects .....	21
Table 4: Four images of the IDEAL algorithm which was used to scan subject TF03 ...	22
Table 5: Mask Segmentation based on Gray values .....	26
Table 6: Create a 3-D model from the Mask .....	27
Table 7: Create STL Models for Export .....	28
Table 8: Modeling Internal Anatomy.....	30
Table 9: Assembly of the Residual Limb .....	31
Table 10: Design method of transferring landmarks to CANFIT for transtibial model rectification .....	38
Table 11: Design method of transferring landmarks to CANFIT for transfemoral model rectification .....	40
Table 12: Overview of creating the FE model options.....	42
Table 13: Major anatomical tissue interaction (contact) matrix.....	46
Table 14: Extended contact matrix – TF03 case .....	51
Table 15: Linear Isotropic material properties .....	58



## **Introduction**

This report details the activities of the two-year Medical Image Generated Dynamic Prosthetic Socket Project undertaken collaboratively by the Georgia Institute of Technology, Emory University and the Georgia Tech Research Institute. The overall goal was to investigate the methods by which prosthetic sockets are fabricated in order to ascertain methods to improve the process for fabrication as well as the ultimate fit of the sockets to the residual limbs.

This report has been formatted to communicate the lessons learned during this project while also serving as a user's manual to some extent so that those interested in investigating, recreating or refining any aspect of this project will be readily able to do so. As such, many of the sections contain tables and figures that walk the reader step by step through the processes.

### ***Background/Problem Statement***

It has been long recognized that the most significant and critical aspect of any artificial limb is the socket—that part into which the residual limb is inserted in order to create an intimate connection between the human and the artificial limb designed to replace his/her missing anatomy. While the sophistication of prosthetic components has been rapidly improving over the last two decades, the fact remains that if the socket does not fit comfortably, the wearer will reject the prosthesis regardless of the components attached thereto.

When reduced to basic elements, the process for constructing artificial limb prostheses consists of four steps: residual limb model acquisition, positive model rectification, prosthetic socket fabrication & fitting. The current practice behind each of these steps is heavily dependent on practitioner and technician experience with little scientific or evidentiary support.[3]

The subjective nature of socket design is based upon prosthetists' experience and feedback from the wearer. Current methods for acquisition of residual limb models only take into account surface topography and, if hand casting is employed, surface palpation of the underlying structures. The exact location of the anatomy, the quantity

and quality of skeletal and soft tissue structures cannot be ascertained through current residual limb model acquisition techniques. Furthermore, a method to quantify socket fit is lacking.

Because of the reasons mentioned above, a scientific approach to socket synthesis does not exist. This project aimed to explore currently available diagnostic imaging techniques, modeling software, computer aided design/computer aided manufacturing software and finite element analysis software packages. Our overall goal was to create a fast and automated prosthetic socket design tool utilizing MRI data for shape acquisition, RL modeling and FEA for model rectification, which will ultimately generate the quantitative properties of a dynamic prosthetic socket.

## **Objectives**

Specifically, this project aimed to:

1. Develop a model acquisition protocol utilizing a Magnetic Resonance Image (MRI) of a person's residual limb (RL) for the initial model. This included both transfemoral (above the knee) and transtibial (below the knee) amputations.
2. Develop a protocol that would rectify the MRI acquired model by applying tissue density properties to the unique soft tissue structures of that RL so that a computer aided design (CAD) socket can be fabricated for that individual.
3. Test the fit of the CAD socket through instrumented gait analysis (IGA) and RL/socket interface pressure mapping.
4. Utilize the MRI model, CAD socket model and data gathered from the IGA and pressure interface mapping to generate a Finite Element Analysis (FEA) model of a dynamic prosthetic socket.

This project was conducted through collaboration between The School of Applied Physiology (AP) at the Georgia Institute of Technology, The School of Aerospace (AE) Engineering at the Georgia Institute of Technology, The Georgia Tech Research Institute (GTRI), and the Division of Musculoskeletal Imaging (MI) in the Department of Radiology at the Emory University School of Medicine

## Approach

### ***Non-Deformation Shell***

Based upon the procedure outlined by Douglas, *et al*[4], and Buis, *et al*[5], a plaster containment shell was fabricated in order to retain natural, non-deformed shape of the residual limb throughout the scan as the subjects would be required to lie on a gantry during their scans. The plaster cast was formed over the residual limb with the subject wearing the gel liner used with their normal prosthesis. A waist belt (for transtibial applications) or shoulder strap (for transfemoral applications) was attached to secure the plaster cast and to simulate minimal loading the limb during the scan. A trans-tibial subject is shown wearing the cast in Figures 1 & 2.



**Figure 2: Lateral view of Subject TT1 in the non-deformational shell**








**Figure 1: Anterior view of Subject TT1 in non-deformational shell**

### **Fabrication of the non-deformational shell**

A description of the fabrication process for a transfemoral non-deformational shell follows in Table 1. The process for fabrication of a transtibial shell is identical with the exception of utilizing a waist belt instead of a shoulder strap. The waist belt consists of an adjustable belt utilizing polypropylene buckles and a 2" elastic suspension strap which descends to the anchor strap. The descending elastic strap also has Velcro® to allow for a secure attachment.

		
<p>Step 1: A liner is selected for the subject based upon their current system or the type of liner anticipated to be utilized during the subjects' fitting and walking trials.</p>	<p>Step 2: The liner is protected with a plastic parting agent. The plastic is wrapped around the waist in order to provide anchorage of the wrap and to protect clothing.</p>	<p>Step 3: Plaster bandage is applied distally to proximal. In this example, the Ossur X5 Seal-In Liner™ is being utilized. Care is being paid to identify these rings in the shell.</p>
		
<p>Step 4: Plaster bandage continues to be applied proximally.</p>	<p>Step 5: Once all the plaster is applied, the ischial tuberosity is palpated so that it can be identified in the shell. Lateral View.</p>	<p>Step 6: Once all the plaster is applied, the ischial tuberosity is palpated so that it can be identified in the shell. Posterior View.</p>

		
<p>Step 7: The shell is removed from the subject. Marks must be placed on the shell to include their ID number, date and a reference line for directly anterior which will be used for the belt installation. Superior View.</p>	<p>Step 8: The suspension component consists of a 1' anchor strap with a buckle and a 5' – 6' long shoulder strap with hook and loop Velcro® to allow for secure fastening. With the shell on its posterior side, the shoulder strap is wrapped into the shell. Anterior View.</p>	<p>Step 9: On the posterior side, the anchor strap is wrapped into the shell. A custom polypropylene buckle was fabricated to allow for MRI compatibility and strap adjustability.</p>
		
<p>Step 10: The completed non-deformational shell.</p>	<p>The buckle measures 2 ¾" wide and 3" high. It has two ¼" x 2 ¼" slits cut into it to accommodate the 2" webbing.</p>	

**Table 1: Fabrication of the non-deformational shell**

The shell was designed to prevent RL distortion while lying on the gantry of an MRI scanner. In the event a stand-up MRI scanner is utilized, this process will need to be tested in order to determine the necessity of the shell or if modifications or refinements are needed.

## ***MRI Scanning***

### **Residual Limb Scanning Background**

Various modalities of medical imaging have been used to derive anatomical models of a lower extremity amputee's residual limb. Volumetric imaging modalities such as Computed Tomography (CT), Magnetic Resonance Imaging (MRI), or ultrasound, allow for the generation of a patient specific three dimensional (3-D) digital models of limb anatomy. These models capture a snapshot of both the residual limb shape and the structure of the underlying tissues. This information about residual limb specific anatomy, such as bone structure or fat/muscle distribution, facilitates improved custom prosthetic limb socket design using CAD/CAM tools and FEA simulation[1].

A number of previous studies have employed X-ray CT scans of the residual limb to obtain models of the limb shape and underlying bone structure. Smith and Vannier performed CT scans on a sectioned human cadaver leg to assess the viability of patient specific modeling of limbs[6]. Zachariah, Sanders, and Turkiyyah assessed the feasibility of CT based patient specific limb modeling using existing CT datasets (from previously scanned amputees) to avoid exposing human subjects to ionizing radiation[7]. Shuxian, Wahhua, and Bingheng utilized CT scans of volunteer subjects to develop 3-D digital models of the residual limb shape and underlying bony structure. In the latter study, the resulting digital model was limited to bony structure contained within undifferentiated soft tissue[8]. Peery, et al, generated a CT based model of a trans-tibial residual limb in a prosthetic socket and attempted to differentiate soft tissue structures[9]. The resulting soft tissue structures were as greatly simplified, to nearly cylindrical, concentric, layers of muscle, fat and skin encompassing the bone. Although CT scans generally produce adequate image quality for simplified limb modeling, one major drawback is the radiation hazard from X-rays. Because of this hazard, the patient generally cannot (or should not) be rescanned if the CT images do not possess adequate soft tissue differentiation for more detailed modeling.

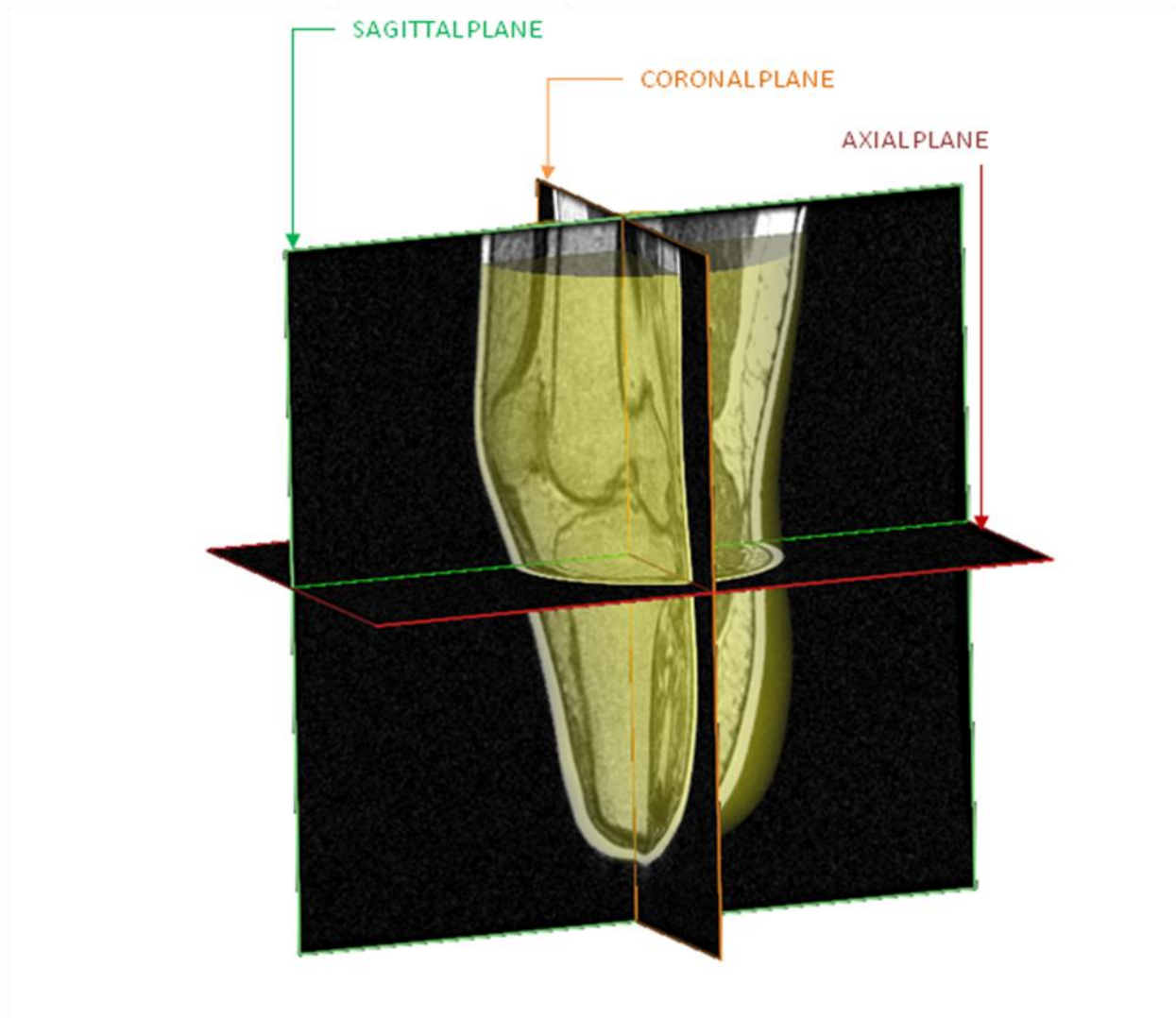
Ultrasound and MRI offer the possibility to obtain models with improved differentiation of soft tissues while not exposing the subject to ionizing radiation. Douglas et al, demonstrated a custom ultrasound scanning device for residual limbs as

an inexpensive scanning option [10]; however, this custom equipment is not universally available. MRI is a commonly available, albeit expensive, imaging modality offering similar benefits. MRI has been successfully employed to generate detailed models of residual limb anatomy in several previous studies [4, 5, 11] and is known to produce excellent soft tissue differentiation.

MRI is a volumetric imaging modality based on excitation of hydrogen nuclei in water bearing tissues to a high energy state using a strong magnetic field. When the magnetic field oscillates, the nuclei alternate between high and low energy states, emitting radio waves in the process. These radio emissions are received by the scanner and spatially reconstructed into an image of the internal tissue structures. Planar images are reconstructed at regular intervals, from slices of within a volume encompassing the anatomy. Signal intensity detected at a point in space is encoded as a grayscale value, ranging from black for an absence of signal to white for the most intense return.

Each pixel records the detected radio emission at the corresponding point in the scan volume. Tissue at any spatial location can be differentiated by the encoded grayscale intensity. However, unlike CT images, the tissue types cannot be readily calibrated to specific grayscale values in the image sets. Different excitation profiles and different methods of image reconstruction result in different grayscale intensities for a tissue types. Furthermore, the grayscale intensity of a tissue type can change with location in the scan volume. Local contrast in gray values denotes a difference in tissue type.

The full set of image slices comprises a tomographic dataset of the scanned volume. This is a discrete approximation of a 3-D volume, consisting of a stack of slice images constructed in the axial, sagittal or coronal planes of the anatomy. This tomographic dataset is typically stored as a stack of digital images in the DICOM 3.0 format. A 3-D model is generated from the image set by interpolating surfaces through selected pixels in adjacent image slices. An example 3-D reconstruction is shown against the typical image planes in Figure 3.



**Figure 3: Orientation of planes with representative scan for TT01**

### **Overview of Scan Series**

A research protocol involving MRI imaging of multiple trans-tibial and trans-femoral residual limbs on volunteer subjects was approved by the Georgia Tech and Emory University Institutional Review Boards (IRB). Residual limbs of six adult patient subjects were scanned by MRI. Three patient subjects were scanned for each class of lower extremity amputation, trans-tibial (below knee) and trans-femoral (above knee). Each scan provided a tomographic image set of limb shape and internal anatomy, from which the limb was reconstructed in 3-D.

Patient positioning and MRI imaging parameters were optimized during the sequence of patient scans, resulting in the recommended procedure in the subsequent



sections. Each class of amputee required a different set of scan parameters to obtain an image set suitable for modeling. Two scanning sessions were required to obtain suitable images of the first patient subject in each class. A series of scans were conducted with different coils, fields of view, and reconstruction parameters to find the optimal imaging parameters. Scans with subsequent patient subjects bracketed these parameters values to find an optimal image. All MRI scans were conducted at Emory Healthcare facilities under the direction of Dr. Michel Terk, Department of Musculoskeletal Radiology, Emory University School of Medicine.

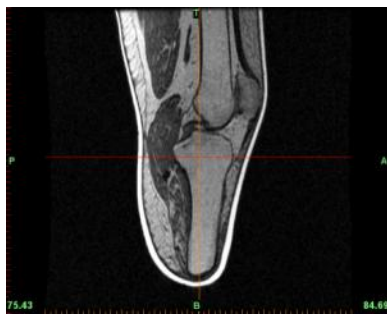
MRI scans were conducted on GE Signa HDx 1.5T and Signa HDxt 3.0T scanners. Pilot scans of the first patient subject (TT-01) were conducted on a GE Signa HDx 1.5T scanner; these were deemed to have insufficient contrast for modeling purposes. All subsequent scans were performed on GE Signa HDxt 3.0T scanner proved, and proved suitable for modeling. Scans of all six patient subjects were scheduled and conducted on the GE Signa HDxt 3.0T scanner.



**Figure 4: GE Signa HDxt 3.0T scanner**

### Trans-tibial Scanning Protocol

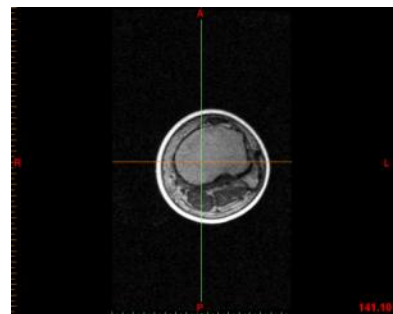
Two sessions of pilot scans were performed with first amputee subject (TT-01) to explore various MRI scanning options. The objective was to determine the approach which would yield the best image contrast and resolution. For all scans, the subject was



**SAGITTAL PLANE SLICE  
(VIEWED FROM LEFT)**



**CORONAL PLANE SLICE  
(VIEWED FROM FRONT)**



**AXIAL PLANE SLICE  
(VIEWED FROM BOTTOM)**

**Figure 5: Sagittal, Coronal and Axial view of Subject TT01**

supine on the gantry, with no gantry tilt, with the residual limb extended. The gel liner and plaster non-deformation cast were worn on the residual limb. The patient was instructed to remain still, while pressing the residual limb into the containment cast to contact the distal end of the limb to the cast throughout the duration of the scan. Imaging slice distance, overlap and reconstruction resolution were varied to find the combination producing the best image quality. Generally, the longer scan times generated better image quality. High resolution scans with excellent contrast were obtained using scanning protocols requiring in excess of 10 minutes; however, during these long scans patient motion generated in mechanical shift artifacts rendering the scans useless. The final scanning protocol was developed as a compromise between image quality (resolution and contrast) and scan time. Reduction of scan time was sought in an effort to mitigate mechanical shift artifacts. Scan acquisition in the sagittal plane, as opposed to the axial plane, significantly reduced scan time significantly by reducing the number of image slices necessary to capture the extents of the residual limb. Albeit lower resolution, this approach still provided adequate image quality for detailed reconstruction of the internal tissue structures of the residual limb.

In the final protocol, the anterior to posterior extents of the scan were, nonetheless, affected by chemical shift, or a change in the MRI return values for a given tissue. Examples of MRI image artifacts encountered in the pilot scan sessions include mechanical shift artifact and chemical shift artifact.

A *Mechanical Shift Artifact* results from patient motion during the scan. The artifact is manifest as a serrated edge along the limb. This is due to patient motion combined with interleaved slice acquisition. This type of artifact was minimized by restraining the patients' residual limb and minimizing scan time. See Figure 6.

A *Chemical Shift Artifact* is a change in the grayscale value of a tissue type depending on spatial position in the scan. This is evident at the extreme ends of the scan value, due to loss of signal at the edges of the coil; significant differences in the grayscale value of bone marrow in the tibia and fibula are noted, as well as a general loss of return at the top of the scan. This type of artifact is minimized by increasing the field of view. See Figure 7.




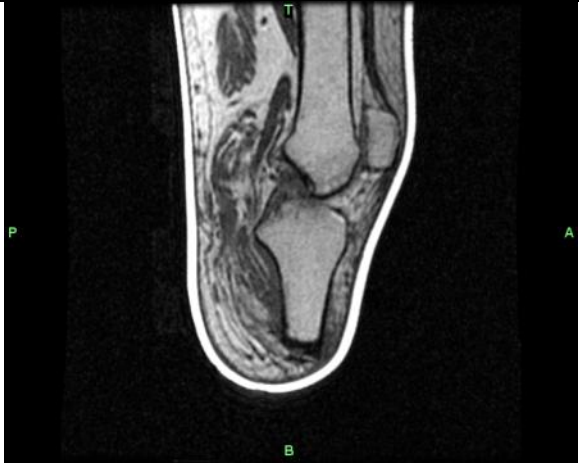
**Figure 6: Mechanical Shift Artifact in TT subject**



**Figure 7: Chemical Shift Artifact in TT Subject**

The final trans-tibial residual limb scan protocol employed a GE Medical Systems Signa HDxt 3.0 Tesla MRI at the Emory Orthopedics and Spine Center facility in Atlanta, GA. The scanning protocol captured the extent of the residual limb, from >10 cm above the femoral epicondyles, to beyond the distal end of the limb. The scan was conducted in the sagittal plane with a 28.0 -30.0 cm field of view, and 1.6 mm slice thickness, and no overlap. Images were reconstructed with 3-D inversion, fast spoiled gradient pulse sequence (FSPGR), with a 256 x 256 matrix. The scan was exported as a DICOM 3.0 image set.

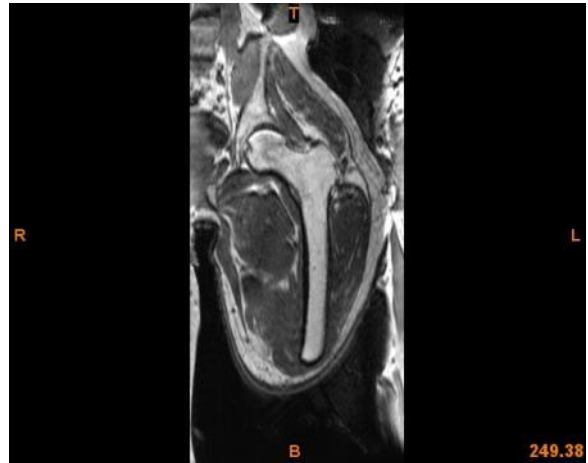
An example slice image from the data set of each trans-tibial subject is shown in the following table. Different soft tissue can be clearly differentiated; fat is denoted by a bright return, muscle denoted by a medium gray return. Cortical bone and tendons provide little to no return, thus appear black in the image. Outlines of the cortical bone are contrasted buy the bright return of the bone marrow contained within the cortical bone outline. The gel liner is easily differentiated from the skin, having a bright return like fat, while the skin return is similar to muscle. A chemical shift artifact can be noted brightening at the extreme anterior or posterior of the limb. The plaster non-deformation shell cannot be detected in the scan.

	<p><b>Subject TT-01</b></p> <p>Imaging Mode: 3D  Pulse Sequence: 3D FSPGR  Imaging Plane: Sagittal  Acquisition Matrix: 256 freq, 256 phase</p> <p>Body Coil  28 cm Field of View</p> <p>1.6mm slice thickness  0.547 mm pixel pitch</p>
	<p><b>Subject TT-01</b></p> <p>Imaging Mode: 3D  Pulse Sequence: 3D FSPGR  Imaging Plane: Sagittal  Acquisition Matrix: 256 freq, 256 phase</p> <p>Body Coil  28 cm Field of View</p> <p>1.6mm slice thickness  0.547 mm pixel pitch</p>
	<p><b>Subject TT-03</b></p> <p>Imaging Mode: 3D  Pulse Sequence: 3D FSPGR  Imaging Plane: Sagittal  Acquisition Matrix: 256 freq, 256 phase</p> <p>Body Coil  30 cm Field of View</p> <p>1.6mm slice thickness  0.586 mm pixel pitch</p>

**Table 2: Examples of MRI scans of the Transtibial Subjects**

## Trans-femoral Scanning Protocol

Two scanning sessions were conducted with the first trans-femoral subject (TF-01) to determine a scanning protocol which would provide suitable image quality. In the first scanning session the patient was positioned both supine and on the side of the intact limb. The first set of images was affected by wrap artifacts, appearing as a reflection of adjacent anatomy into the field of view. An example



**Figure 8: Example of a wrap artifact on a transfemoral subject scan**

of the wrap artifact is shown in Figure 8. The wrap artifact was addressed by modifying patient position and increasing field of view. All three trans-femoral subject scans proved to be unique cases. Ultimately, a different scanning approach was employed for each trans-femoral subject however the position that was preferred was side lying on the unaffected side. The objective in each scanning session was to capture the full volume of the limb with good contrast to noise ratio, while minimizing artifacts.

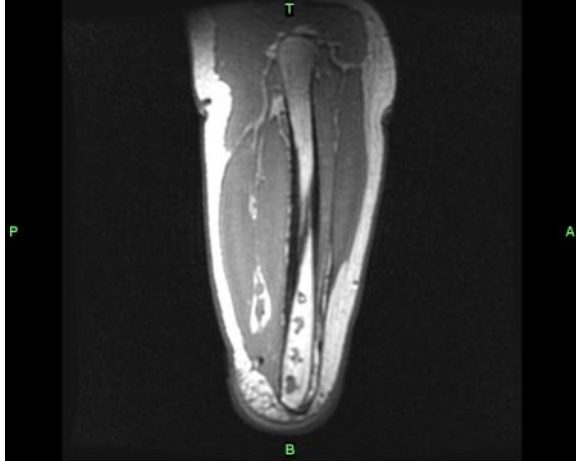
Chemical shift artifacts can be noted in the example images from the selected studies subjects TF-01 and TF-02 (See Table 3). The chemical shift presents a significant challenge in differentiating and segmenting tissues. Of note for both of these cases is the fact that they have very long residual limbs.



**Figure 9: Example of TF01 Subject lying on his unaffected side with his legs strapped to assist with keeping them still**



**Figure 10: Example of TF01 subject lying on affected side for scan. This produced a wrap artifact.**



### Subject TF-01

Imaging Mode: 2D, T1  
 Pulse Sequence: FSE-XL  
 Imaging Plane: Sagittal  
 Acquisition Matrix: 192 freq, 192 phase

Body Coil  
 48 cm Field of View

2 mm slice thickness, 0.5 mm spacing  
 0.938 mm pixel pitch



### Subject TF-02

Imaging Mode: 3D  
 Pulse Sequence: FSPGR  
 Imaging Plane: Sagittal  
 Acquisition Matrix: 192 freq, 192 phase

Body Coil  
 42 cm Field of View

1.8 mm slice thickness  
 0.820 mm pixel pitch

**Table 3: Representative scans of the TF 01 and TF 02 subjects**

### The IDEAL MRI Algorithm

An optimal protocol may have been found when scanning the last trans-femoral subject (TF-03), the GE IDEAL algorithm. IDEAL is an MRI algorithm released in 2007 for use on the General Electric Signa HDxt3.0T MRI scanner. This algorithm provides four image sets from a single acquisition; these image sets provide multiple contrasts: fat-only, water-only and combined fat/water in-phase and out-of-phase images. Furthermore, this imaging algorithm is less susceptible to chemical shift artifacts. This image set proved ideal for modeling purposes. Images from Subject TF03 using the IDEAL algorithm are found in Table 4. Chemical shift artifacts are not evident in the image sets generated using the IDEAL algorithm.

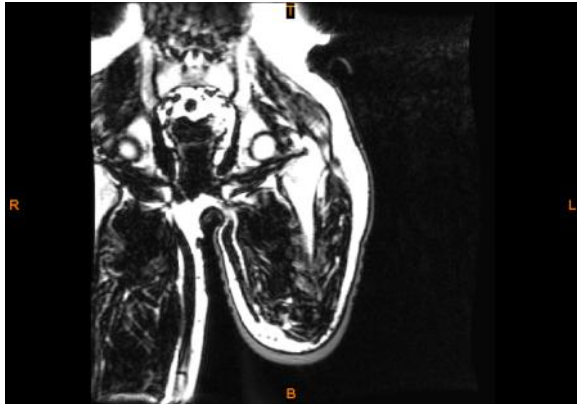


**Subject TF-03**

Imaging Mode: 3D  
Pulse Sequence: SPGR  
Imaging Plane: Coronal  
Acquisition Matrix: 320 freq, 192 phase

Body Coil  
48 cm Field of View  
4.0 mm slice thickness

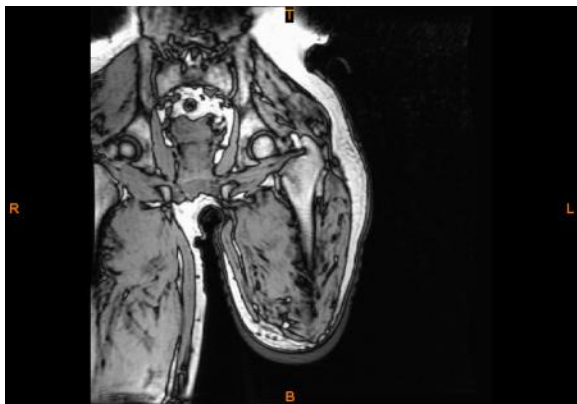
TT-03 Image A: Fat Only



TT-03 Image B: Water Only



TT-03 Image C: Fat/Water In Phase



TT-03 Image D: Fat/Water Out-of Phase

Table 4: Four images of the IDEAL algorithm which was used to scan subject TF03

## Segmentation & Modeling

Patient specific three dimensional digital models of residual limb anatomy were reconstructed from the DICOM datasets using Materialise MIMICS. MIMICS is a medical image viewing, manipulation package, and model reconstruction software application for Windows based workstations. Over the duration of the project several versions of MIMICS were employed, starting with V12.1 and ending with Version 14.0. The MIMICS graphic user interface is depicted in the following figure, showing the modeling of a residual limb gel liner from an MRI data set.

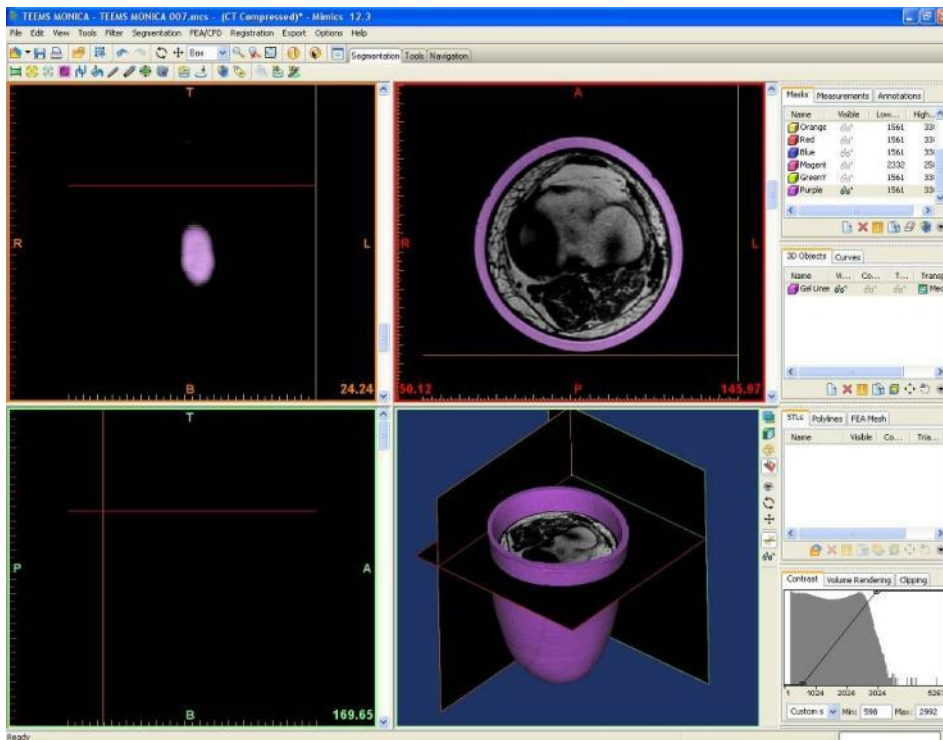


Figure 11: MIMICS user interface showing a TT residual limb

Using one or more specialized utilities in MIMICS, the medical image data is segmented into subsets, or masks, encompassing a tissue structure of interest. Each mask is a selected subset of voxels, or slice image pixels thickened to the distance between slices. With the mask defined, MIMICS interpolates surfaces between outer contours of the voxels. Surfaces are interpolated using an implementation of the Marching Cubes Algorithm [12]. In this implementation of the algorithm, local gray value is used to weight the interpolation between the slices to account for partial volume effects in voxels along the boundaries of tissue structure. A triangular patch is

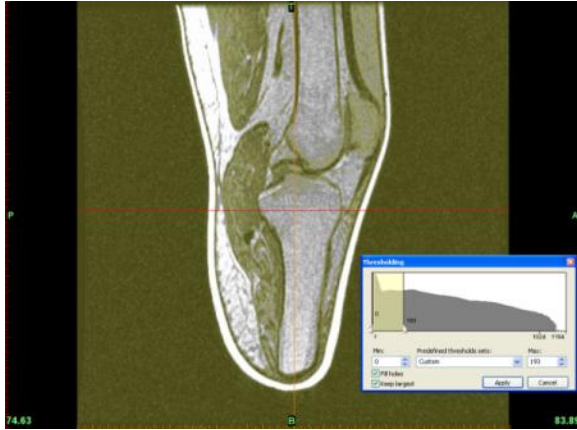


generated which locally approximates the true surface contour. An entire surface of triangles encompasses a volume, defining a three dimensional model of the anatomy segmented in the mask.

The quality and resolution of the image data influence the final accuracy of the derived model. Independent assessments of MIMICS accuracy modeling anatomical structures appears in published literature. For example, Jamali, et al [13], investigated the accuracy MIMICS computer model reproduction of a pelvis by comparison of physical measurements of anatomical landmarks on a standard to software based measurements on the MIMICS model; measurements on the computer model deviated from the standard by a mean of 1.5 mm. Gelaude, VanderSloten and Lauwers concluded that 3-D model of a human femur generated by MIMICS deviates by half the maximum voxel dimension, or the defining resolution of the medical image set [14].

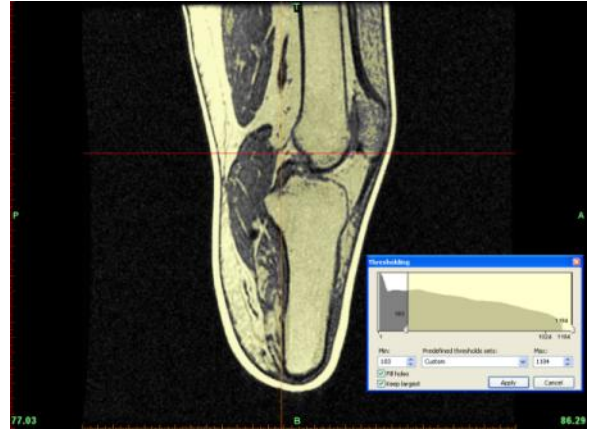
The volumetric model generated by MIMICS is structurally equivalent to the STL model universal STL 3-D model format. The STL model is an efficient format to represent complex three dimensional forms. Furthermore the STL model is defined, explicitly, in three dimensional space; thus, the geometric relationship of anatomical STL models, generated from the same medical image set, is inherently defined and maintained. MIMICS provides several utilities to refine and optimize the 3-D model for simulation and manufacturing purposes. Furthermore, starting with MIMICS V14.0, a direct link is provided to the Materialise 3matic STL manipulation application. Within 3matic, the STL models can be used as the basis for computer aided design or prepared for Finite Element simulation.

The following section outlines the modeling of a residual limb from MRI images using MIMICS. The section is broken into five distinct tasks. The first task is **Mask Segmentation based on Gray values** and it is detailed in Table 5. The second task is to **Create a 3-D model from the Mask**. This task is detailed in Table 6. The third task related to segmentation and modeling the residual limb is to **Create STL Models for Export** the details for which are found in Table 7. The fourth task is **Modeling Internal Anatomy** (Table 8) and finally **Assembly of the Residual Limb** (Table 9).



**Step 1:** Pixels in a slice image are segmented into subsets using the “Segmentation” tool in MIMICS. The mask encompasses all pixels of a selected gray value range in the dataset, selected pixels are shown in yellow. Successful modeling requires sufficient contrast to isolate the tissue of interest.

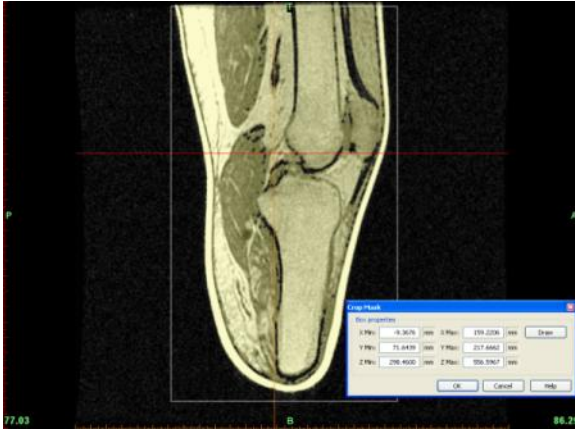
In the case of MRI images created by an SPRG algorithm, air, cortical bone, muscle and tendons will generally be captured in the lower gray value range, as shown in the figure to the left.



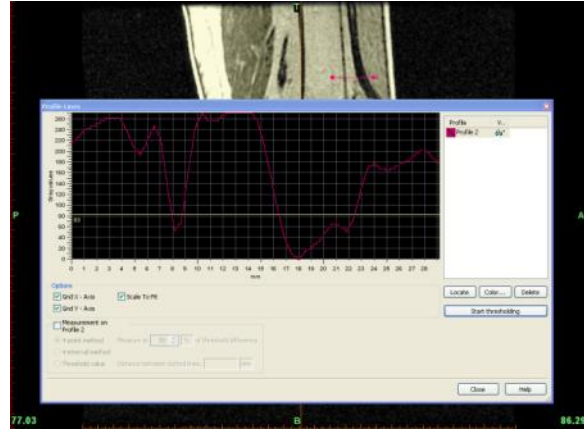
**Step 2:** Higher gray values typically capture issues with greater lipid content, such as fat or bone marrow; as shown in the figure to the left. The subject’s mineral gel liner comprises the highest return values, seen as the bright ribbon around the limb. In most scans the gray values for a given tissue type or anatomical structure are not consistent across the entire image slice. As shift in the intensity of gray values in the fat can be seen where the posterior values are aft structures lighter than the anterior. Likewise, a general loss of contrast from muscle to bone is noted.



**Step 3:** This example will produce a model of the entire limb volume, which will serve as the limb shape for socket design. The MIMICS “Segmentation” tool is used to select a gray value range that captures the majority of the pixels comprising the leg, while excluding noise in the airspace. The blue pixels highlight that external noise can be picked up if the gray value range is set too low in an attempt to capture tendons and bone within the limb. The proper gray value range is a judgment call for the modeler. This mask is segmented globally from the entire image set. If necessary, overall image contrast to noise ratio can be improved by applying digital image filters from the “Filter” menu in MIMICS.



**Step 4:** A basic approach to eliminating noise or unwanted tissue structures in the mask (pixel subset) is to limit the region of the mask in the image dataset using the “Crop Mask” tool in MIMICS. The range of interest can be limited to a three dimensional region defined by a bounding box. The bounding box is adjustable in all three slice views (coronal, sagittal, and axial). Once set, the mask will be limited to the defined region; however, the global segmentation range cannot be modified. The mask is now named and saved.



**Step 5:** The saved mask can be filtered in a number of ways to insure that the pixel subset encompasses only the tissues of interest. First, using the “Region Growing” tool, the mask can be further filtered to only the pixels connected to a region of interest. This can be done in a single slice, or globally across all slices, where connection of adjacent pixels can be detected.

Measurements of distances and grayscale variations in an image are useful in deciding how to further filter the mask. The image to the left is a measurement of grayscales and distance across a gap in the mask.

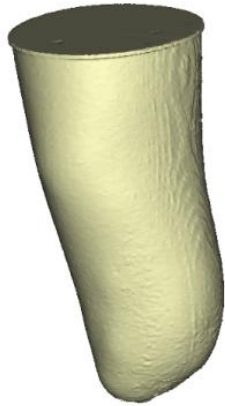


**Step 6:** Filters which can be applied to the mask set include:

- Morphology filters based on digital 3-D topography
- Region growing combined with image morphology
- Localized gray value segmentation
- Manual pixel editing on the slice level

Gaps in the mask, shown to the left, were eliminated using the “Close” morphology operation. The filter first dilates the mask subset by adding pixels to the edges in each slice, then only retains the added pixels which touch each other along multiple edges. The effect of this filter is to close three dimensional gaps in the mask, without changing the overall shape.

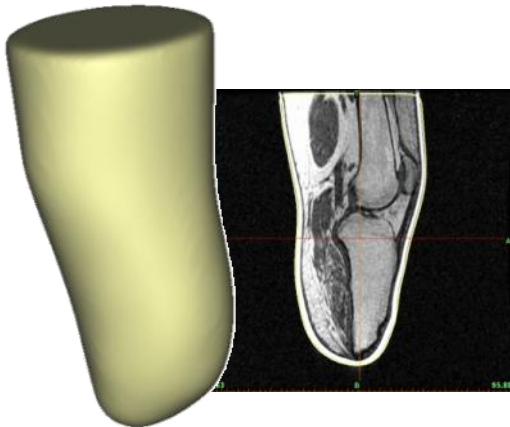
**Table 5: Mask Segmentation based on Gray values**



**Step 1:** A three dimensional surface model can be generated from any mask (pixel subset) spanning two or more contiguous image slices. The surface is computed in MIMICS using the “Calculate 3D” tool. This tool interpolates between the contours of the mask in each image slice using the Marching Cubes Algorithm<sup>##</sup>. The result is a tessellated 3-D model, using many triangular surface panels to approximate the shape. The image to the left is a rendering of the limb external shape from the mask set in the previous section. Some defects related to the interpolation algorithm are evident as bumps and scalloping on the surface.



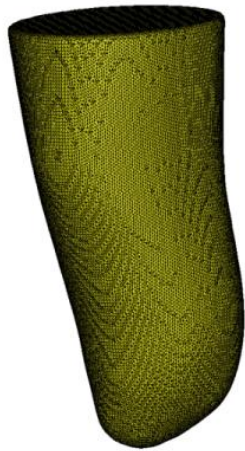
**Step 2:** Quality of the 3-D model and accuracy to the contours of the medical image slices can be assessed by displaying the 3-D surface contours over the original images. Yellow surface contours in the figure to the left show an internal void and some slight deviation of the 3-D surface from the limb shape. These problems can be addressed either by editing the mask and re-computing the 3-D surfaces or refining the 3-D surface using the “Wrap” or “Smoothing” tools.



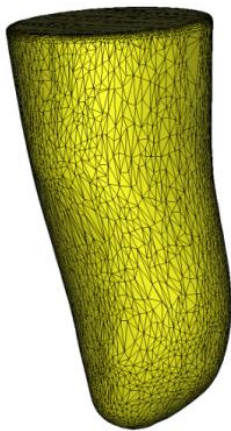
**Step 3:** The “Wrap” tool smooths and closes surface gaps in the 3-D model, but at the same time reducing detail and dilating the model. The “Smoothing” tool acts similar to a noise filter, averaging away small asperities in the surface. Smoothing generally gives in a more accurate and realistic surface contour, but may lead to a minor volumetric shrinkage of the model or hole.

As shown in the figure to the left, the rough surface of the original 3-D model of the limb was eliminated using a combination “Wrap” set to a smallest detail level of 2mm. This was followed by “Smoothing” (2<sup>nd</sup> Order Laplacian, factor = 0.9, 10 iterations) until the surface contours closely match the limb outline in the slice images.

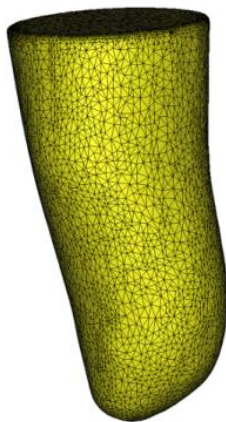
**Table 6: Create a 3-D model from the Mask**



**Step 1:** The end product of the modeling procedure is generation of an STL digital model for use in simulation, socket design, and automated manufacture. The 3-D model produced by MIMICS is in the tessellated structure of an STL model, and need only be exported in the explicit STL file format. However, the triangulated structure of this model is generally not suitable for use in simulation without additional processing. A typical STL triangle surface structure of a MIMICS model is shown in the figure to the left, this is the smoothed and wrapped model of the limb with the triangulated structure displayed. The surface structure still retains artifacts of the noise present before the smoothing operations, and is comprised of thousands of triangles.



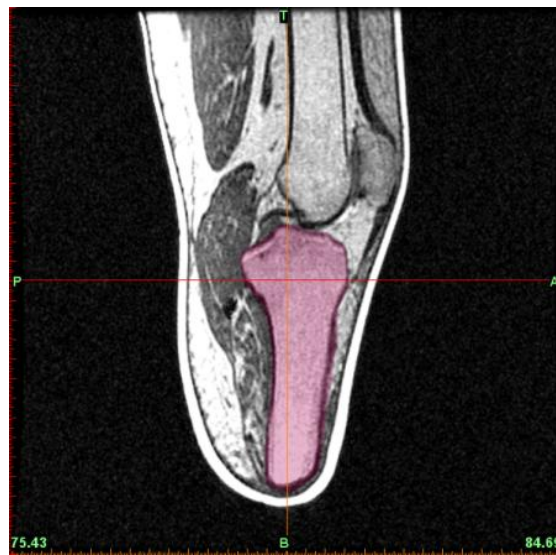
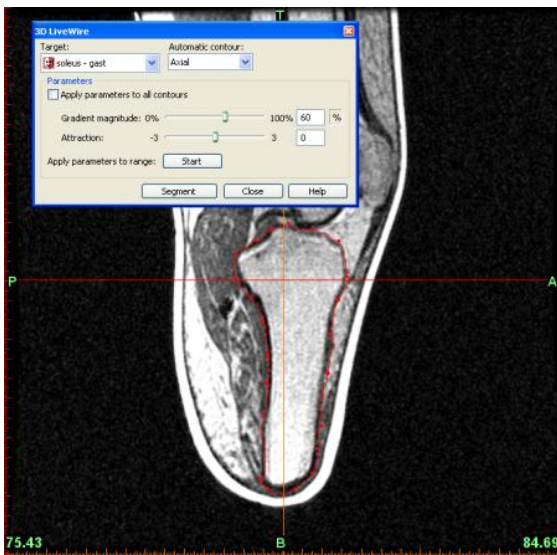
**Step 2:** The triangulated surface approximation can be optimized using the “Triangle Reduction” and “Remesh” tools in MIMICS. In the Figure to the left, “Triangle Reduction” was applied using the advancing edge algorithm. Ten iterations were run at a tolerance of 0.1mm and edge angle of 2. The new triangle structure is nearly free of all scalloping from previous surface artifacts. Furthermore, the number of triangles was reduced by an order of magnitude, while maintaining a surface fidelity to within 1/5 of the minimum pixel dimension. However, the surface is comprised of a number of narrow, high aspect ratio triangles, which are not suitable for simulation.



**Step 3:** As a final step, a re-meshing of the surface is performed, using the “Remesh” tool; this utility is launched in 3matic directly by MIMICS. The “Remesh” utility optimizes the triangulated surface, eliminating the high aspect ratio triangles, while maintaining a specified tolerance to the original surface. The optimized triangle mesh is shown in the figure to the left. This optimized version of the limb was exported in binary STL format using the “STL+” utility in MIMICS. This version is of the limb shape is suitable for use in socket design and for to support detailed modeling of the of the limb’s internal anatomy.

Table 7: Create STL Models for Export

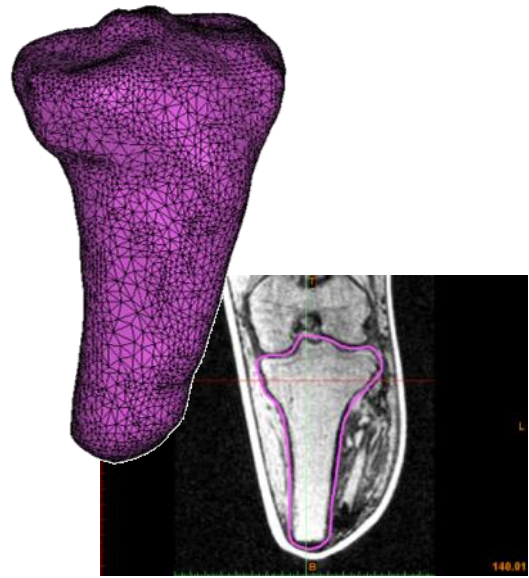
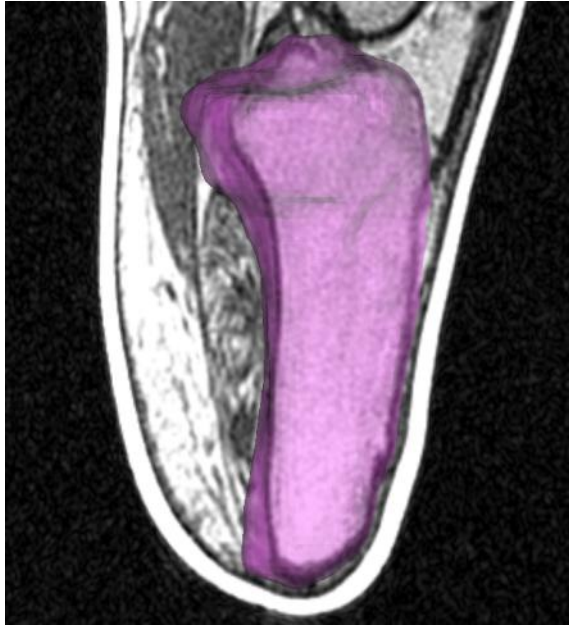
Modeling the internal tissue structure of the limb follows the same general procedure as outlined for obtaining an STL model of the limb shape. The major difference is that more sophisticated mask segmentation techniques are often required to obtain an accurate model. Most tissue structures are composed of several distinct ranges of gray values, which are not easily distinguished from adjacent tissues, especially in cases of low image contrast or contrast to noise ratio. More sophisticated segmentation approaches are required to generate these models. The following is a general outline of a modeling approach; however, in practice each model required some unique steps based on the experience of the modeling engineer.



**Step 1:** Boundaries of internal anatomical structures were often defined by the gradient in grayscale values from adjacent anatomy, as opposed to a narrowly defined band of grayscale values. Often it was not possible to define a mask by conventional segmentation. However, the mask could be defined in a number of other ways. A powerful approach, introduced in MIMICS 13.0, is the “*Live Wire*” tool. This tool provides semi automatic detection of contours based on gradient in grayscale values. A contour is formed around the region of interest by tracing the contour and adding anchor points as shown above. Contours are traced in a number of slices on two orthogonal planes, and a guiding wireframe is automatically computed.

**Step 2:** The resulting mask spans all of the slices contained between the boundaries of the wireframe. Manual editing of the mask is necessary to capture any areas that are excluded, or erroneously included in mask region.

The resulting mask is depicted in the single sagittal slice image to the left, the pink highlighted pixels show the mask selection. Here the masked pixels cover a wide range of gray values, from nearly 0 in the cortical bone of the tibia, to over 300 in the marrow. Gray values in adjacent muscles and fat overlap these values, precluding a simple segmentation.



**Step 3:** A 3-D model is computed from the mask following the same procedure outlined in the previous example. The 3-D model is superimposed on the sagittal slice image in the figure to the left using the “Toggle Reference Planes” viewing mode and solid transparency. It is often useful to use this visualization mode as a quality control check to insure that all of the anatomy has been captured in the 3-D model. In addition, the contours of the 3-D model can be compared to the slice images, as described in the case of the external limb model.

The “Optimal” setting is recommended for initial generation of a 3-D model from the mask. Smoothing and wrapping can be applied as a secondary step. If the contours do not match the slice images, a custom 3-D interpolation can be generated. In the latter case it is recommended to switch the interpolation algorithm to “Contour” before adjusting any other settings.

**Step 4:** The resulting 3-D model must be wrapped and/or smoothed as previously described for the limb. These procedures must be followed by a triangle reduction and remeshing, as necessary to obtain a suitable surface. In general, the surface should be comprised of primarily equilateral or near equilateral triangles, with the minimum density required to maintain a maximum tolerance of 20% of the smallest pixel dimension. In the example case, the smallest pixel dimension in the image set was 0.57mm; therefore, a tolerance of 0.11 mm, or better, is desired for the 3-D surface. As a final quality control check the contours of the 3-D model should be compared to the original slice images.

**Table 8: Modeling Internal Anatomy**



**Step 1:** Modeling of the residual limb generally proceeds as follows:

- STL Models of the bones and major ligaments are produced using the procedures previously outlined.
- An STL model of the subjects' gel liner (if present) is generated.

These are generally the least complex geometry and easiest structures to segment and model from the MRI dataset.



**Table 9: Assembly of the Residual Limb**



**Step 2:** Next, models of the muscles are generated by advanced mask segmentation techniques, including:

- Live Wire
- Morphology Region Growing
- Local Thresholding
- Manual mask editing

3-D models are created from the masks. The 3-D model surfaces are generally crude and require extensive application of Wrap and Smoothing before export as an STL. The STL models of the muscles are matched to the bone models by a Boolean subtraction of the bone model from the muscle models, eliminating overlapping regions.

**Step 3:** The skin and fat are generally the most complicated geometry to extract. As opposed to the normal segmentation, this model is obtained by Boolean subtraction of the other STL models from the original STL model of the entire limb. The result of the described Boolean subtraction is shown in the figure to the left.

The resulting geometry is often quite complicated and contains geometric features unsuitable for FEA simulation. Further manipulation is thus required before generating the FEA mesh. The details are provided in the section on FEA simulation.



## CAD Socket Design

The anatomical model of the residual limb and gel liner, generated in MIMICS, is used as the basis for design of prosthetic socket variants. STL models of the tissue structures and the gel liner are exported from MIMICS, retaining spatial relationship. Design of prosthetic limb socket is performed using the modeled internal anatomy for guidance. Multiple variants of the prosthetic socket design can be generated in the digital CAD environment. These designs can then be evaluated by FEA simulation or, if deemed a satisfactory, used to manufacture of a socket mold pattern.

A starting surface shape definition of the residual limb is extracted from the gel liner STL model, as described in the previous section, this starting shape model is analogous to the plaster casting of the limb made by the prosthetist in traditional fitting procedures. Modifications, or *rectifications*, are made to the starting shape in software. Two CAD approaches were explored:

- Direct manipulation of the limb shape STL in 3matic
- Export of a the limb shape STL to a standard prosthetics design application

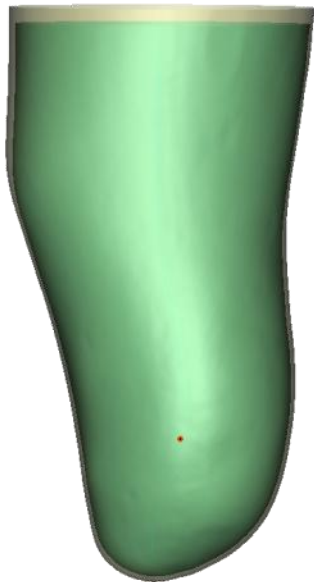
Using 3matic allowed for direct manipulation of the external limb shape STL, referencing the internal anatomy as a guide to perform rectifications. This approach, while ideal for modifications proved extremely difficult to implement due to limitations in the software to allow for the modifications to be completed, thus an alternative approach was pursued using CANFIT (Vorum Research Company, Vancouver, Canada) prosthetics software. The major drawback to using CANFIT was the inability to import more than one STL model into CANFIT, making it impossible to directly reference the internal anatomy.

A work around solution was developed to solve this problem by applying anatomical landmarks on the limb surface shape with small indentations (using 3matic) which related to the underlying anatomy of interest. Thus the marked STL file could be exported for manipulation to CANFIT software with the relevant anatomy identified and the orientation maintained. Once the file was rectified in CANFIT, it would then be converted into an STL for export. An outline of each approach is provided in the following sections.

## Socket Design using 3matic

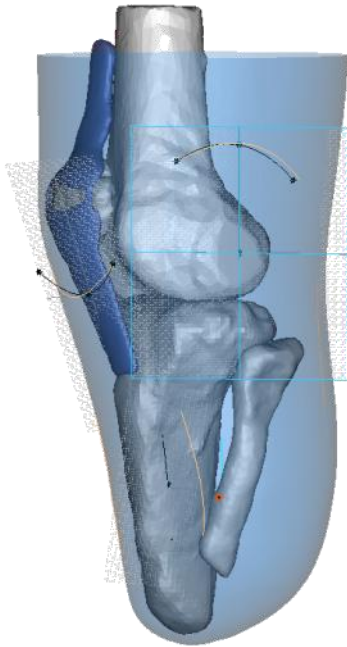
A Patella Tendon Bearing Below-Knee Prosthesis, or PTB, socket design was generated for subject TT-01 using solely using 3matic. The rectifications are applied to the external shape of the limb, generating the inner surface shape of the PTB socket. The typical PTB design and rectifications are detailed in a classic reference report by Radcliffe and Foort [15]; these include reliefs and protrusions necessary to suspend the socket on the residual limb, or to relive pressure points in sensitive areas on the limb.

To obtain the starting shape for the socket, the outer surface of the gel liner STL model is copied to a new part. Next, the part is smoothed and refined to eliminate surface imperfections, using smoothing and remeshing tools in 3-matic. Finally, the triangle density of the surface increased to facilitate surface morphing operations. Shape modifications, or rectifications, are applied to this prepared model of the limb shape.

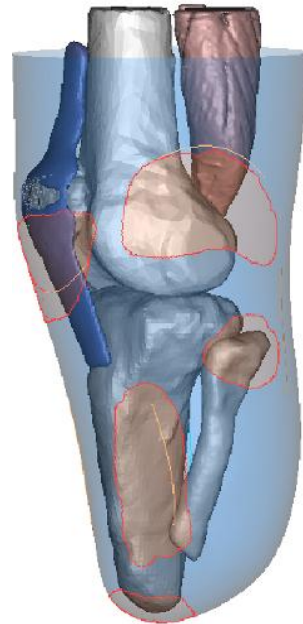


**Step 1:** The first morphing operation is a *ply reduction*, or volumetric reduction of the starting limb shape. To perform this operation, a suitable center point for a uniform scaling operation is necessary. A centerline spline through the residual limb shape is generated and 3-D points are placed along the centerline spline. Trial ply reductions are performed using these points as center points for uniform scaling, until a nearly uniform offset of the original surface was obtained, as shown in the figure to the left. Typical ply reductions are on the order of 10% of the original limb volume, and are necessary for comfortable fit and proper walking gait.

In the model to the left, the original is shown in tan, the modified model in green.



**Step 2:** The hard tissue anatomy of the residual limb and the patella tendon STL models are imported in the original spatial relationship to the gel liner model. These structures are visualized under the underlying reduced surface shape using the transparency renderings in 3-matic. Next, sketch planes are positioned on the anatomical structures at the locations normally identified by palpitation of the patient; the origin of each plane is positioned at the exact anatomical landmark location, parallel to the local surface. Rectification guide markings, as outlined in Radcliffe and Foort [15] are drawn on these planes, as shown in the accompanying figure above.



**Step 3:** The rectification guide markings are projected to the surface of the reduced starting shape as attached curves. The length of each curve is tailored as necessary for a particular socket design variant. Next, surface regions to be modified are selected using the marking tools (shown in orange).

Unnecessary anatomy can be temporarily hidden in order to simplify the review of the rectifications.

Additional rectifications include loading above the medial and lateral condyles of the femur (on the upper sides of the socket), loading either side of the tibial crest (on the lower anterior of the socket) and loading the patellar tendon.

Reliefs, or build ups are added over the distal tibial end and the fibular head.

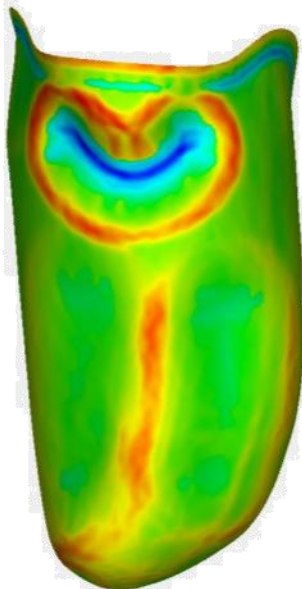
It is necessary for these rectifications to be smooth for the comfort of the wearer, so smoothing operations are performed on the rectified socket and checked with curvature analysis tools in 3matic.



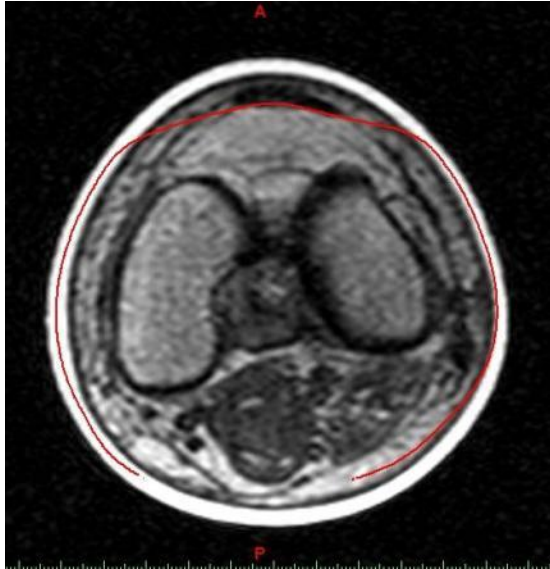
**Step 4:** Surface morphing tools are employed to create reliefs and protrusions on the surface. Most apparent rectification is the deep groove under the patella, or the Patella Tendon Bar (ref. the figure to the left). The position and extents of this groove are governed by the shape of the patella and the length of the patellar tendon, easily identified in the 3-D model.

The biggest unknown here is the extent to which each modification should be made.

Of note here is that the tendon appears to protrude through the rectified socket. This is the result of the patella bar which will ultimately be loading the patellar tendon.



**Step 5:** The figure to the left shows a curvature analysis on the surface of a completed socket design, indicating some additional smoothing around the Patella Tendon Bar rectification may be necessary before the design is finalized.



**Step 6:** Comparison of the rectified socket geometry to the internal anatomy can reveal possible areas where additional rectification is necessary. This assessment can be performed on the 3-D geometry in 3-matic, or an STL of the rectified socket shape can be exported for comparison to the reformatted MRI slices using MIMICS, as shown to the left. The red outline of the socket shape is superimposed over an axial reconstruction of the MRI dataset.

Herein lays the beauty of having digital access of underlying anatomy.

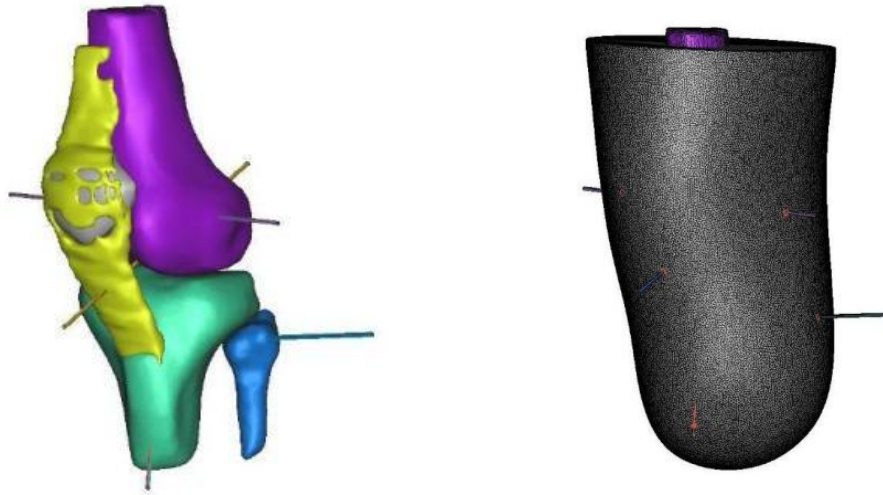


**Step 7:** An example of a rectified socket design is compared to the original starting socket shape in the figure to the left. Once the rectifications are considered satisfactory, the resulting surface is exported as an IGES surface patch set using 3-matic CAD Link. This surface model is then used as the socket inner surface definition in FEA simulation and as a positive mold shape definition for manufacturing the socket. Positive mold patterns manufactured from the digital socket design can be used to produce thermoformed polymer trial sockets for patient fit checks, or can ultimately be used as mandrels for carbon fiber lay-up of a final, definitive socket for delivery to the patient.

### Socket Design using CANFIT – Transtibial Models

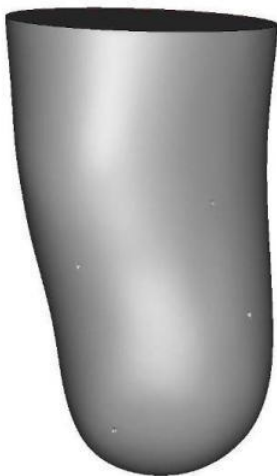
The CANFIT prosthetics design software was used as the design environment to produce PTB diagnostic sockets for all three trans-tibial subjects. This approach provided the prosthetist with a familiar design environment, dedicated to the design and modification of prosthetic sockets. However, only the external shape of the limb could be imported into the CANFIT design software. CANFIT did not allow for the import and display of multiple STL files; thus the internal anatomy of the limb could not be directly referenced to guide the socket design. 3-matic was still necessary to perform initial STL

preparation, file conversion, and specific steps necessary for check socket pattern manufacture. All Diagnostic sockets tested on subjects were produced by this process. The process is summarized in Table 10:



**Step 1:** The positions of internal anatomy of interest are marked by normal projections from the anatomical landmarks. This function is performed in 3-matic, using the STL models of the internal anatomy of the limb (bones and tendons). The markings projected from the anatomy are saved as a single STL file.

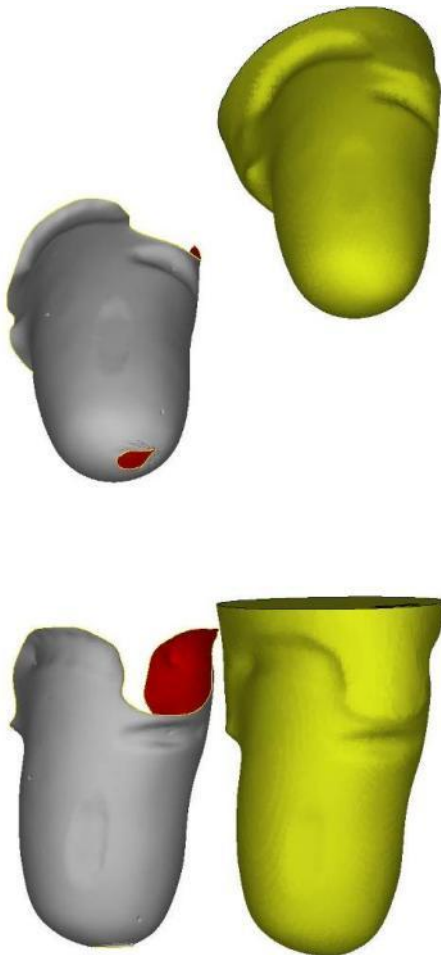
**Step 2:** The STL model of the residual limb shape is superimposed over the internal anatomy in 3-matic. The projections of anatomical landmarks to the gel liner surface are marked with surface points. Next, 2-4mm deep dimples are inscribed into the surface of the gel liner model at the marked points, using the carve tool in 3-matic.



**Step 3:** Resolution of the residual limb surface STL model is optimized for modification. Next, the STL model is rotated from the supine orientation of the MRI scan into the standing coordinates (this orientation is expected by the CANFIT design template, and necessary for proper import). The rotation consists of a 90° rotation about the transverse axis of the limb, followed by a 90° rotation about the centerline of the limb. The marked and rotated model of the gel liner was exported from 3-matic as an STL file, and imported into CANFIT.



**Step 4:** Modifications to the limb shape (rectifications) are performed in CANFIT according to the template for a PTB prosthetic socket. The prepared design is a surface shell representing the inner surface of the intended prosthetic socket. This can include the intended trim lines for the socket (as shown in the figure to the left). The final shape is exported as an STL file from CANFIT.

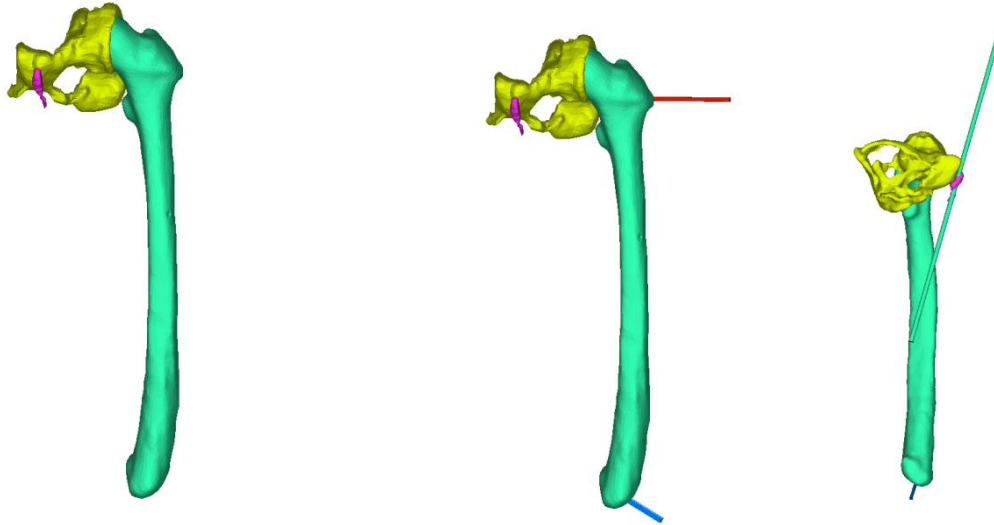


**Step 5:** The CANFIT socket design (gray) is imported back into 3-matic in order to correct surface flaws (holes, surface ripples) and refine the mesh structure of the socket surface. The corrected socket surface shell is exported as in IGES or STEP file for use in FEA analysis. For manufacturing purposes the open shell is closed into a watertight solid, by extending the free edges and lofting the superior edge of the socket shape to a circular or oval termination 20-50 mm above the most superior point on the trim line. Closing the surface in this manner provides a mandrel shape for casting a thermoformed check socket or braiding a final socket. The final socket mandrel shape is shown in yellow. This shape is exported as an IGES file for mandrel carving.

**Table 10: Design method of transferring landmarks to CANFIT for transtibial model rectification**

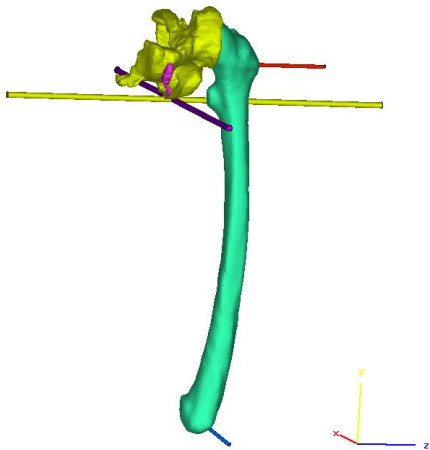
## Socket Design using CANFIT – Transfemoral Models

Process of modification for the transfemoral models followed a similar route. This process is detailed in Table 11.



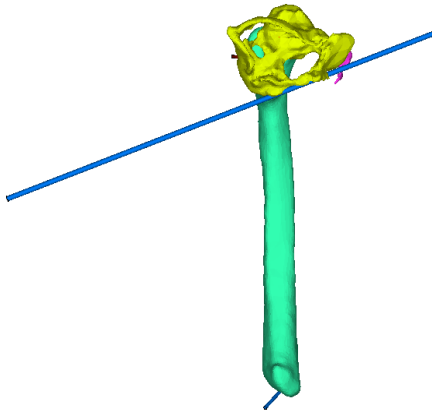
**Step 1:** For the transfemoral models, the initial landmarks are identified through the femur, the adductor longus tendon and the pelvis as captured from the MRI scan.

**Step 2:** Pins are added to identify the location of the greater trochanter and the distal femur. The image to the right identifies the adductor longus.

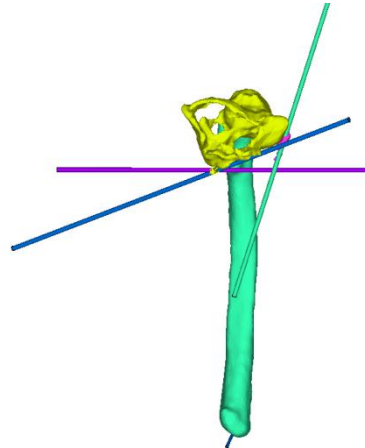


**Step 3:** Pins are added to identify the Ischial level in both the sagittal and coronal planes.

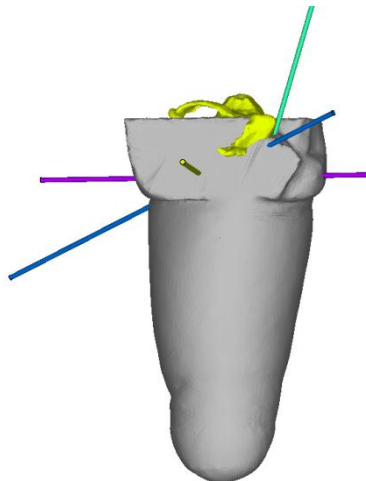




**Step 4:** The last pin identifies the Ischial ramal axis.

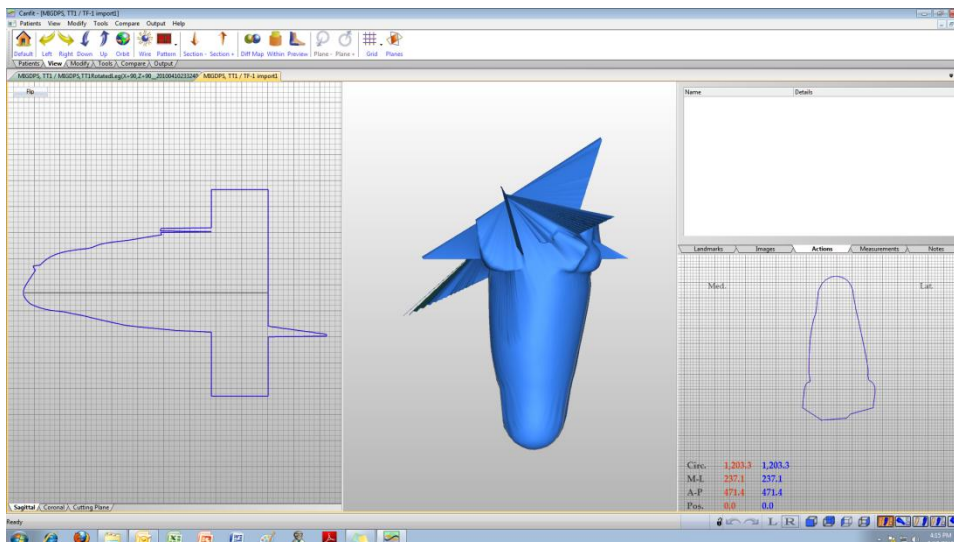


**Step 5:** The image above shows the transfemoral skeletal anatomy with the pins projecting towards the surface of the model.



**Step 6:** Outer surface of the liner is shown with the relevant pins protruding through its surfaces. Hence the planes and anatomical landmarks of interest are precisely communicated to the model. This entire surface, complete with pins is saved as an STL file can is then imported into CANFIT in order to allow for model rectifications.

While the planes create artifacts as part of the importation process, these are easily rectified out and then used accordingly as landmarks.



**Table 11:** Design method of transferring landmarks to CANFIT for transfemoral model rectification

## ***FEA Analysis***

### **FEA Introduction**

Optimized Magnetic Resonance Imaging (MRI) protocol is identified and successfully used to obtain the shape of the residual-limb. In a subsequent step MRI data of the residual limb are imported into *Mimics* medical imaging software. Utilizing *Mimics* digital CAD capabilities MRI slices are transformed into three-dimensional volumetric geometry representing major tissues, i.e. bone, tendon, muscle and fat. This manual provides the detailed steps required to perform Finite Element Analysis (FEA) to simulate prosthetic socket interaction with the residual limb. Patient-specific requirement of the analysis entailed two major challenges, namely, its repeatability and general applicability. Therefore, the FEA is designed based on the principals of computational anatomy in order to attain these requirements. First, repeatability is required to eliminate the need to rebuild the Residual Limb (RL) FEA model every time an analysis iteration is required upon socket model rectification. A simple rule is used to attain the repeatability, a *model developer* (person with advanced knowledge of FEA) will import the anatomical entities “only once” to *ABAQUS* and prepare the analysis, while a *user* (person with minimal knowledge of FEA) will import rectified socket geometry into *ABAQUS* and run the analysis as many times as required to converge to the final design. Second, general applicability is required to guarantee the FEA steps are universal and independent of the specific patient anatomy or amputation location and history.

The outline of these steps is provided in Table I. Only model preparation is performed in *3-matic* (by Materialise) while all other steps are performed in *ABAQUS*. Model preparation starts at importing the three-dimensional volumetric geometry of major tissues (obtained from MRI segmentation) into *3-matic* to obtain CAD representative models in STEP format (ISO 10303) or Initial Graphics Exchange Specification (IGES). *ABAQUS* FEA software is capable of importing STEP or IGES data of major tissue structures as individual parts of the residual limb assembly. Subsequent steps to importing geometries into *ABAQUS* involve meshing, material assignment, assembly, interactions and loading.

**Table 12: Overview of creating the FE model options**

Software	Task
<i>Mimics</i>	<b><i>MRI to 3D volumetric geometry</i></b>
	Segmentation
<b>Finite Element Model Development</b>	
<i>3-matic</i>	<b><i>Model Preparation</i></b>
	Individual anatomical entities
	– Wrap function
	– Smooth function
	– Auto Remesh
	– Quality Preserving Reduce
	Triangles
	Interaction of anatomical entities
	– Boolean CAD operations
	CAD Link export to STEP or IGES
<i>ABAQUS</i>	<b><i>Finite Element Analysis</i></b>
	Import parts
	Generate optimized FEA mesh
	Assign material models
	Assemble model
	Create contact behavior (interaction)
	Assign loading
	Run analysis checks

For demonstration purposes this guide will use example cases independent of the patient case under study to guarantee the generality of discussion. Meanwhile, all FEA steps will be applied to a single patient model (example) to provide a comprehensive discussion.

## FEA Model preparation

### Model preparation, Individual anatomical entities

Segmentation procedures of MRI data performed in *Mimics* results in three-dimensional (3D) volumetric geometries of tissue structures. Figure 1a provides the muscle community above the knee all lumped in one 3D entity as obtained from MRI data segmentation. This 3D volumetric geometry lacks surface smoothness including holes and/or small inclusions as shown in Figure 12-A. These imperfections are filtered out using the Wrap and Smooth functions provided in the *remeshing* module. As these details are filtered out, smooth 3D volumetric geometries of reasonable accuracy are obtained as shown in Figure 12-B. The purpose of filtering out these imperfections is to obtain optimized geometry suitable for numerical analysis. Existing or remaining imperfections in the model may render any FEA impossible since imperfections are major cause for numerical singularities in the mathematical models associated to the analysis. Irregular yet smooth surfaces will result in less than optimal interaction or contact identification between different tissues, and hence drastically increase analysis cost in terms of run time.

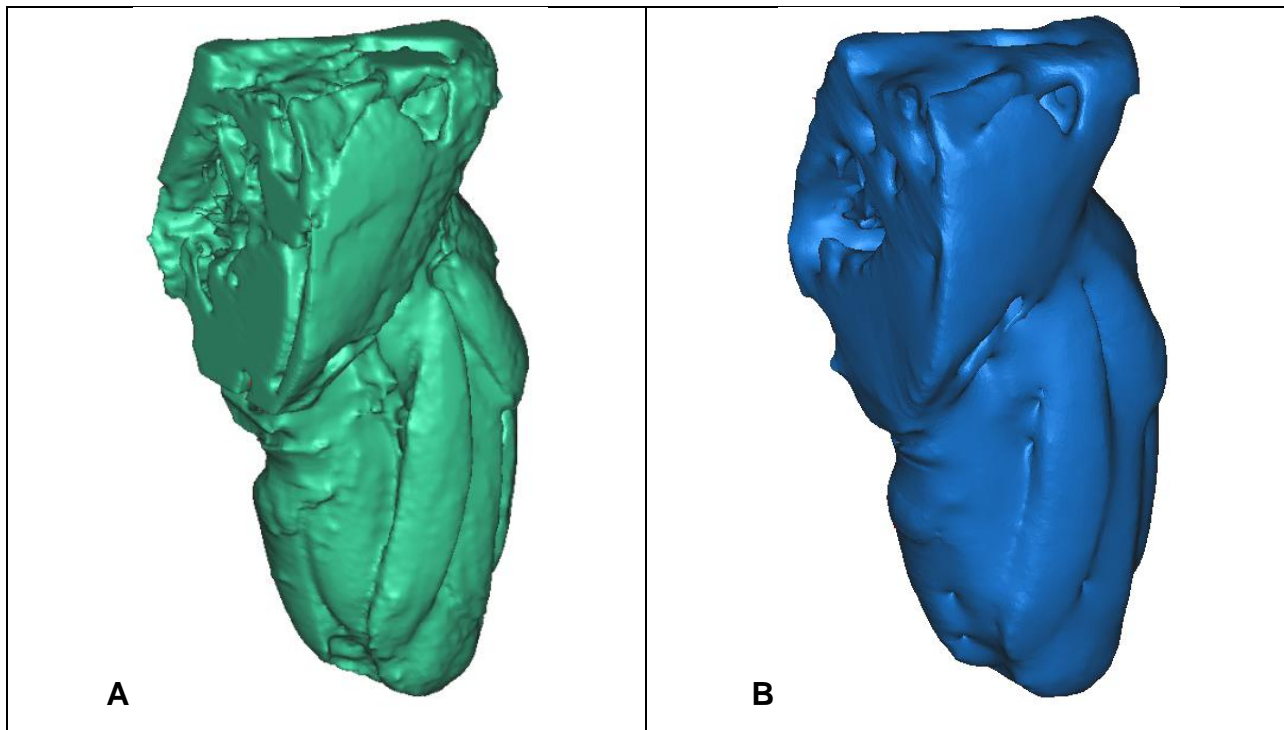


Figure 12: A- 3D geometry as obtained from MRI (left), B- Optimized smooth 3-D geometry (right)

In order to filter out imperfections two *3-matic* functions are used, namely, *Wrap* and *Smooth*. *Wrap* function as described in *3-matic* user manual “*The wrap operation will create a wrapping surface of the selected entities. The wrap function is useful for medical parts, to filter small inclusions or close small holes. Furthermore the function is a useful tool towards Finite Element Analysis, where an enveloping surface is needed*”. Also *Smooth* function will result in enhanced surface geometry in terms of better triangulation of the surfaces by *reducing the noise in the triangulation*. In order to guarantee that a 3D geometric entity will be exported in an optimal size CAD data file two more operations are performed. *Auto Remesh* and *Quality Preserving Reduce Triangles* are designed to optimize the volumetric triangular mesh while maintaining the 3D model accuracy.

## **Model preparation, Interaction of anatomical entities**

In this section the guide utilizes an example of a trans-tibial case in order to illustrate the necessity of the suggested step. Performing MRI segmentation in *Mimics* different tissue types are constructed and their associated surface imperfections and/or inclusions are filtered out. A critical aspect in preparing a computational model is to eliminate overlaps and/or gaps between matching surfaces of adjacent tissues. These gaps and overlaps result from numerical anomalies when *Mimics* is constructing the surfaces through interpolation of sectional and intersectional points. Figures 13 and 14 provide an example of such overlaps between different entities of fat, tendons, bones and muscles. Meanwhile, the Finite Element model requires minimum flaws (gaps and overlaps) of mating surfaces. Therefore, the assembly of the FEA model is prepared in *3-matic* by creating identical mating surfaces of neighboring anatomical entities.

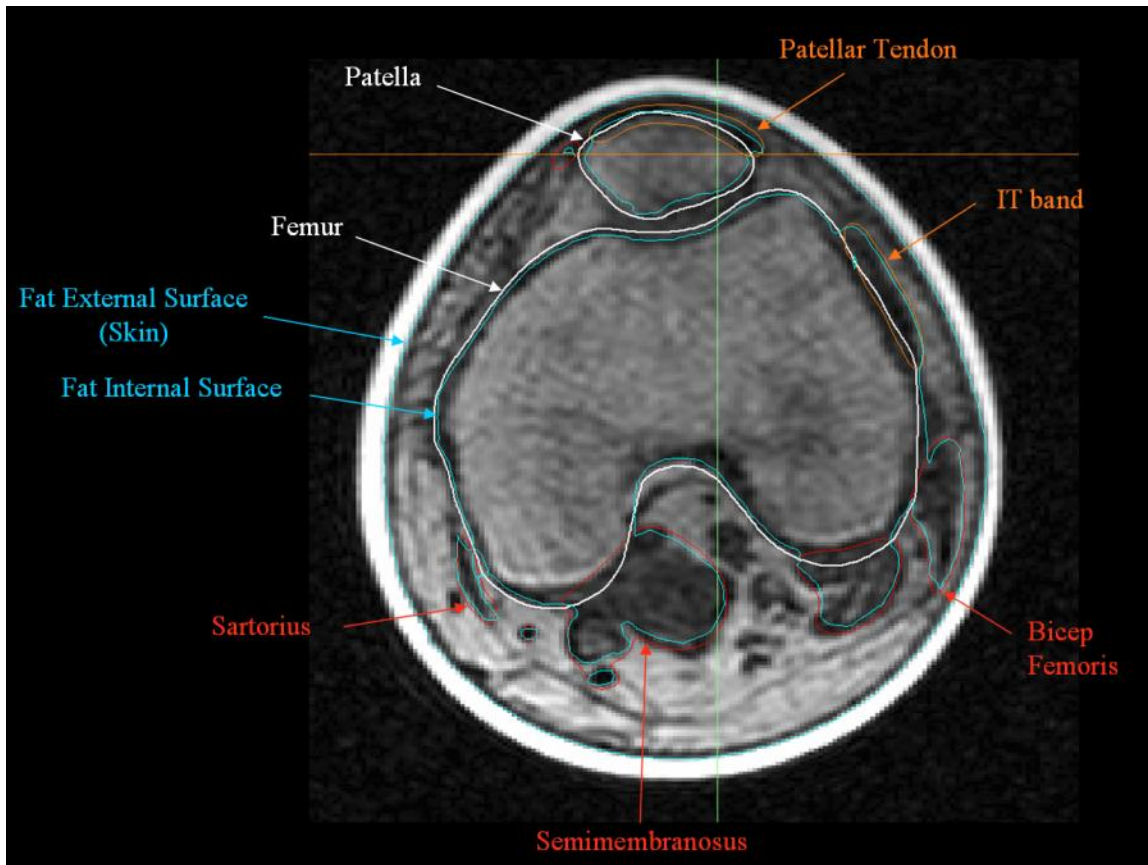


Figure 13: Overlapping boundaries of tissues (section above the knee in a trans-tibial case)

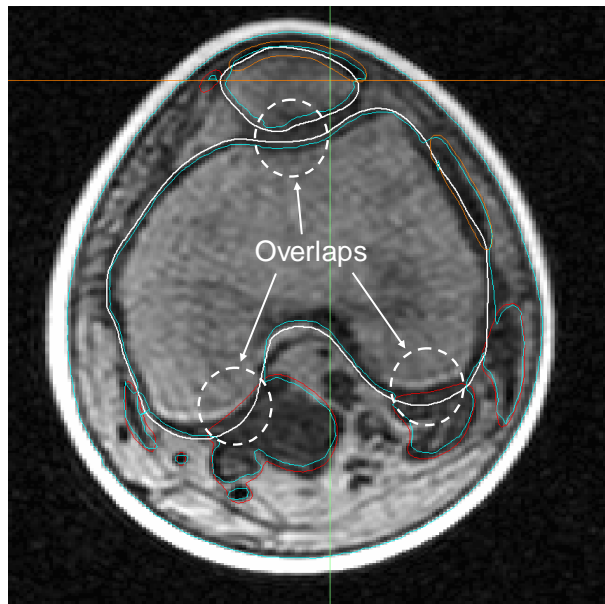


Figure 14: Overlaps between different tissue types

A first step to resolve mating surfaces flaws is to identify major anatomical parts of the model. For the example of a trans-tibial patient analysis major bones are Femur, Tibia,

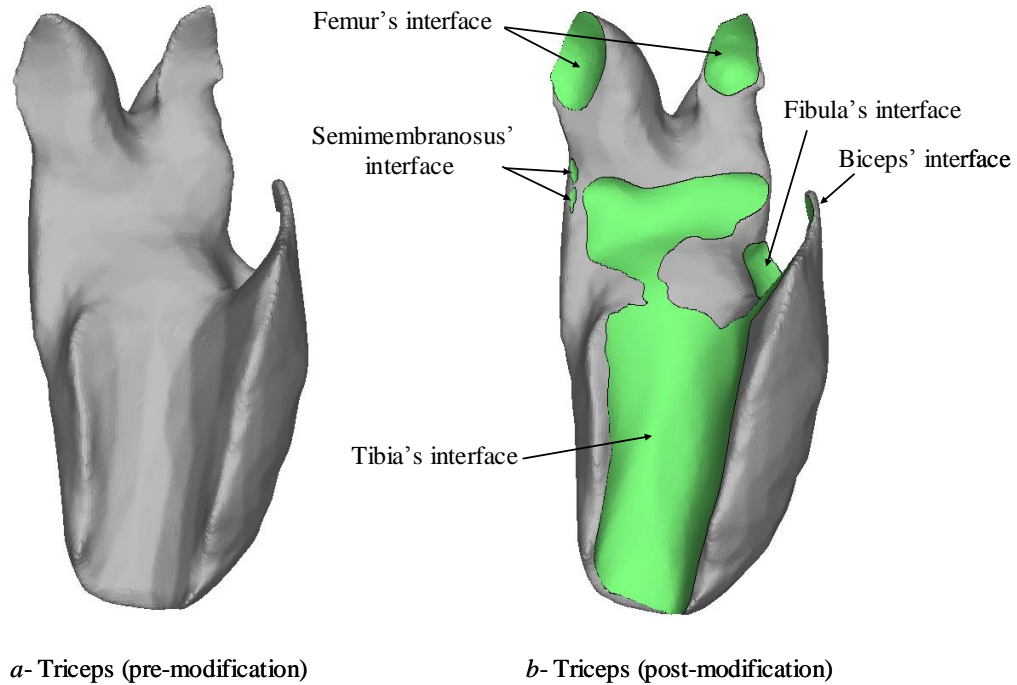
Patella, and Fibula. Major muscles are Quadriceps femoris, Biceps femoris, Sartorius, Semimembranosus and the Triceps surae. Finally major tendons are the Patellar tendon and the Iliotibial band. Table 13 provides the interaction or contact among the formerly mentioned major anatomical parts

**Table 13: Major anatomical tissue interaction (contact) matrix**

Item	Femur	Tibia	Patella	Fibula	Quads	Biceps	Sartorius	Semimem	Gastroc	Pat Ten	IT band
<b><u>Bones</u></b>											
Femur					✓	✓	✓		✓		
Tibia				✓				✓	✓	✓	✓
Patella										✓	
Fibula		✓							✓		
<b><u>Muscles</u></b>											
Quads	✓					✓				✓	
Biceps	✓				✓				✓		
Sartorius	✓										
Semimem		✓							✓		
Gastroc	✓	✓		✓		✓		✓			
<b><u>Tendons</u></b>											
Pat Ten		✓	✓		✓						
IT band		✓									

Fat tissue in a trans-tibial amputee’s case represents further contacts or interactions with all formerly mentioned anatomical parts. Meanwhile, fat as a major tissue type is not mentioned in Table 12 as its geometric model, and consequently its computational model, is constructed through Boolean operation.

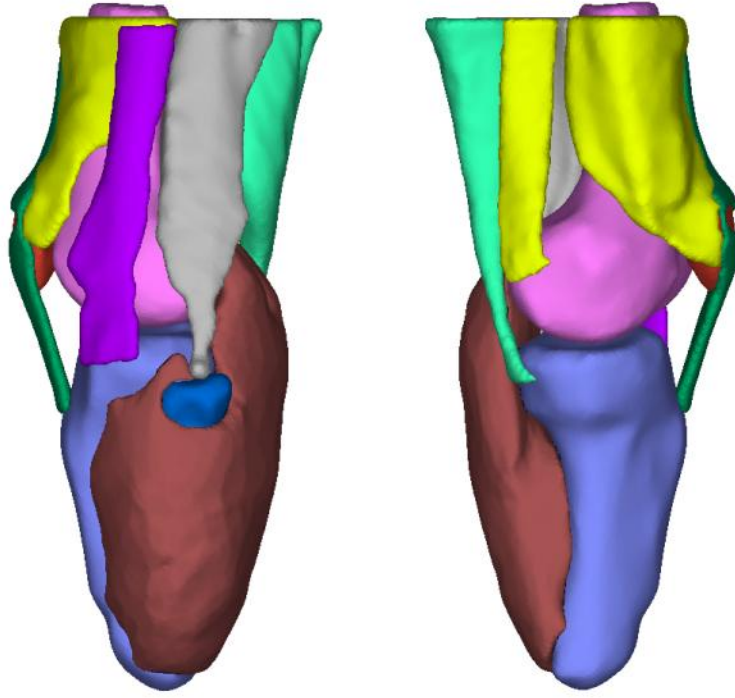
The Triceps Surae is used as an example to demonstrate eliminating interaction flaws. Figure 15 provides the original shape of the Triceps obtained from segmentation (in *Mimics*) together with the modified shape at its interface surfaces with mating tissues. These modifications are obtained in *3-matic* using Boolean subtract operations of surrounding tissues from the Triceps.



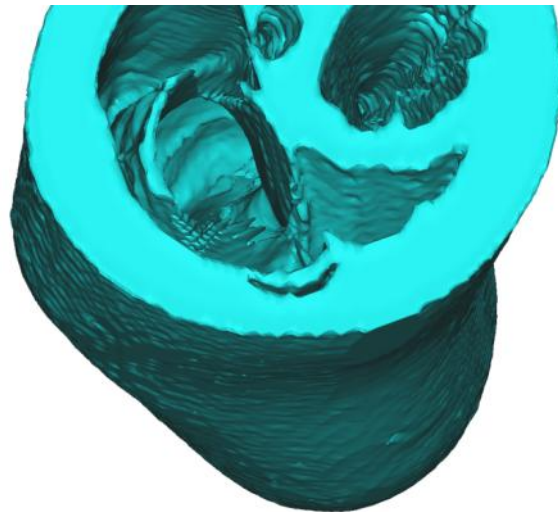
**Figure 15: Modified surface of the Triceps muscle at the interface**

Interaction flaws are removed in each anatomical entity according to the interaction matrix provided in Table II. Afterwards, all major tissue structures are assembled into one object using Boolean union operation as shown in Figure 16. This assembled object is consequently subtracted from the internal surface of the gel liner using a Boolean subtract operation and resulting in the three dimensional geometry of the fat. Figure 17 provides the fat geometry obtained from direct segmentation of the MRI, while Figure 18 provides the product of the Boolean operation to construct the fat. It can be seen in Figure 17 that surface construction is poor consisting of fragments, ridges small inclusions due to the interpolation numerical anomalies discussed earlier. On the other hand Figure 18 provides higher quality surfaces, precise boundaries and most importantly optimum interface with major tissues of the model.

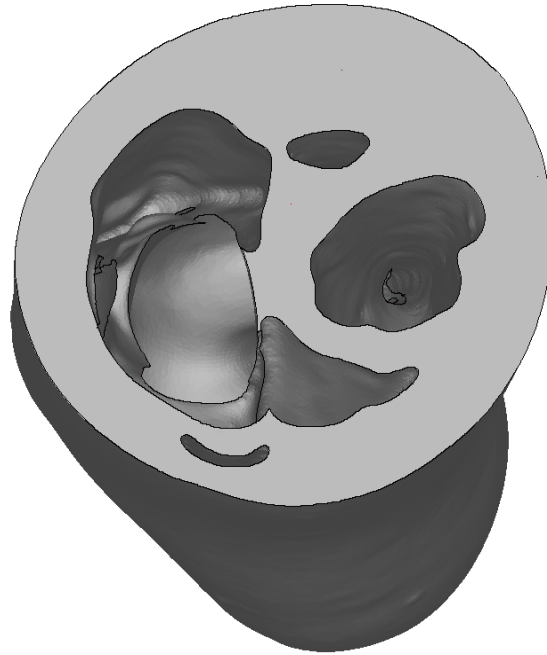




**Figure 16: Assembled bones, tendons and muscles (left leg – lateral and medial views)**



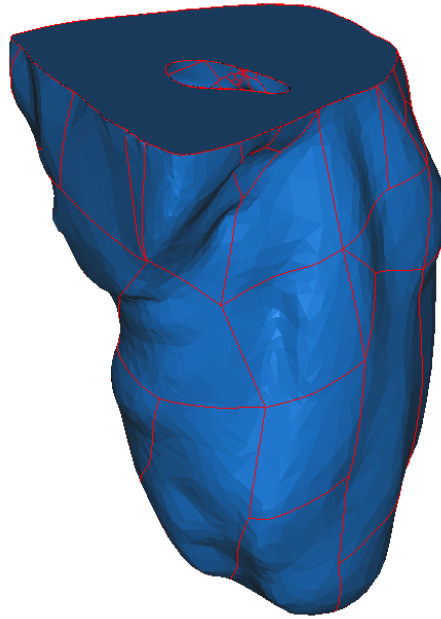
**Figure 17: The 3D geometry of fat tissue as obtained directly from segmentation**



**Figure 18: The final 3D geometry of fat tissue as obtained via Boolean operations**

### **Model preparation, *CAD Link* export into STEP or IGES**

*CAD Link* module in *3-matic* facilitates converting 3D triangular based model description into an analytical representation recognizable by any CAD or FEA software. Resulting analytical representation of the surface are transformed into planes, tabulated cylinders, general surface of revolutions and/or NURBS surfaces (Non-uniform rational b-spline, i.e. freeform). Analytical representation of 3D geometries are exported via the *CAD Link* tool into either STEP or IGES format, both CAD format are readable by ABAQUS FEA software. Figure 19 illustrates the analytical representation of the muscles community above the knee which is to be imported into the FEA software. Different color (red) lines show the boundaries of analytical surface patches in the new analytical representation of the muscle community.



**Figure 19: Analytical geometry of the muscle community as obtained from CAD Link**

When performing the *CAD Link* operation to export analytical representations, *3-matic* provides a feedback report regarding the quality of the export process. In order to guarantee error proof export/import process this feedback should include “zero” errors as shown in Figure 20.

Logger
Reverse Engineering - Result Information
-----
Planes: 1
Cones or cylinders of revolution: 0
Tabulated cylinders: 0
Spheres: 0
General surfaces of revolution: 0
Ruled surfaces: 0
Free-form (NURBS) surfaces: 173
-----
No mesh: 0
Empty mesh: 0
Close mesh: 0
Degenerated mesh: 0
Inconsistent mesh: 0
No unique projection found: 0
Approximation is too complex: 0
Face creation error: 0
Reverse Engineering failed: 0
Reverse Engineering failed: 0
Internal error: 0
-----

**Figure 20: 3-matic Logger feedback report providing the export process quality**

This process of model preparation in *3-matic* is essential for successful FEA of socket interaction with the RL. The process should be performed by an advanced user of the medical CAD software *3-matic*, preferably the same FEA *model developer* or at least with perfect coordination with. This requirement of perfect coordination is implied by the practical flow of tasks and clear understanding of the *3-matic* user of FEA requirements.

## FEA Process

In this section, for demonstration purposes, a trans-femoral model (TF03) is used. The steps were tested in the cases of trans-femoral (TF), trans-tibial (TT) amputation alike and proven both repeatability and general applicability. An FEA *model developer* is to follow the demonstrated steps here within to establish the FEA model for the first time. The FEA model is to be built only once for any specific patient.

The TF03 example model used contains the following major anatomical entities, bones, muscle and fat together with other entities or parts of the gel liner and the socket. All parts belong to 3D geometries SOLID except for the prosthetic socket which belongs to 3D SHELL geometry. The interaction matrix for a TF case is given in Table 14 and obtained by combining all bones into one structure and similarly treating the muscles and the fat. The extended interaction matrix provided in Table III includes non-anatomical entities or parts such as the gel liner and the socket. It must be noted that the skin is not considered in the FEA model. Therefore an interaction between the gel liner and the muscle implies that it takes place across the skin. The assumption of neglecting the skin is justified by the fact that the skin possesses very low strength and hence does not contribute to the load carrying capacity of the RL.

**Table 14: Extended contact matrix – TF03 case**

Item	Bones	Muscles	Fat	Gel liner	Socket
Bones		✓			
Muscles	✓		✓	✓	
Fat		✓		✓	✓
Gel liner		✓	✓		✓
Socket			✓	✓	

## Importing part (individual successive operations)

Important note: *Mimics* and *3-matic* represent the 3D geometry in the same units as the MRI data, i.e. in millimeters. Meanwhile *ABAQUS* FEA software requires the user to employ a consistent set of units across all variables, i.e. length dimensions in meter, forces in Newton and mechanical properties such as Young's modulus in  $\text{Newton/m}^2$ . Therefore, while importing parts into *ABAQUS* the user will scale the part dimension to one hundredth to be in meters instead of millimeters. Erroneous outcomes associated to relative location in space will result in case the user attempts to import the parts in millimeters and scale them down at later step.

Importing the **bones** as SOLID 3D geometry is shown in Figure 21.

Import process: File menu → Import Part

Options: Solid – Stitch edges using tolerance (2 mm)

3D –Deformable

Multiply length by 0.001 (from mm to m)

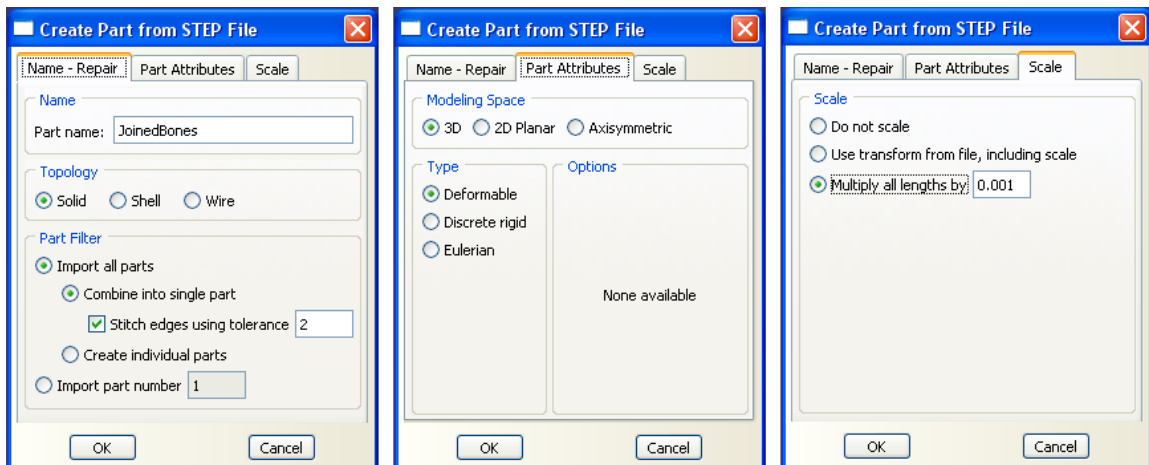
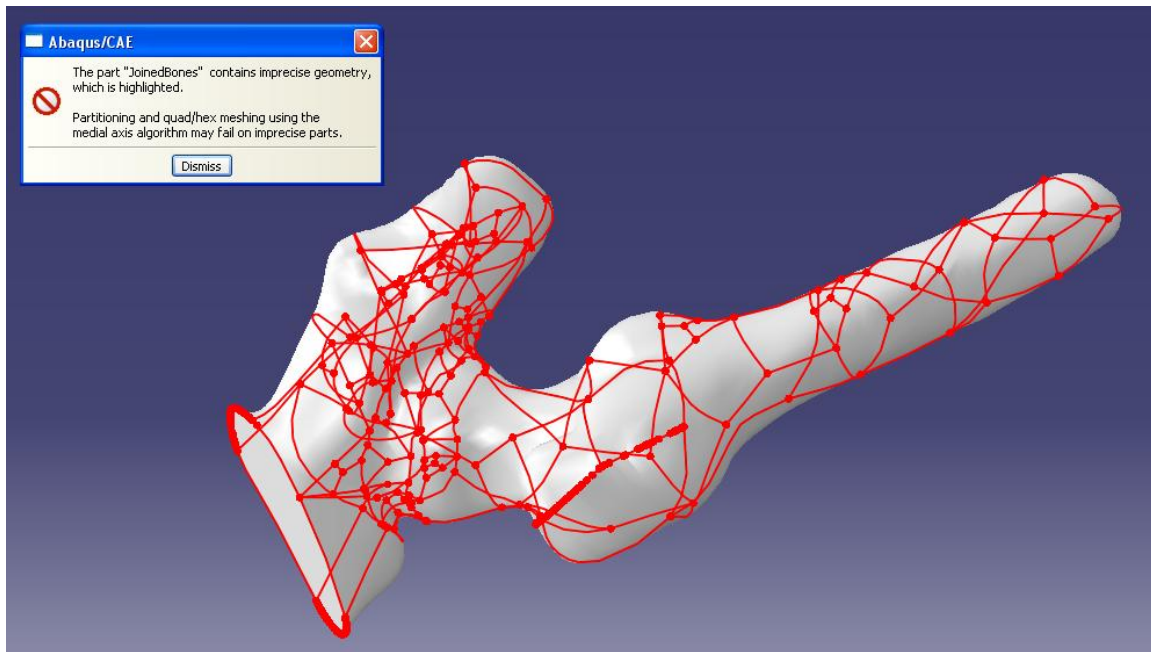


Figure 21: Solid import options

The imported object of the 3D solid analytical geometry of bones is shown in Figure 22 with warnings associated to, imprecise geometry (stitched edges) and partitioning or quad/hex meshing may fail (no need for partitioning and a tetrahedron mesh will be used instead of quad/hex mesh)



**Figure 22: Imported 3D solid analytical geometry of bones**

The user has to verify that the part import was successful as a 3D solid by updating part validity from the part manager. When updating the validity for the 3D solid analytical geometry of bones, the user should obtain a similar message

Part 'JoinedBones' contains valid geometry and topology.  
 Part 'JoinedBones' is a solid part (1 cell, 136 solid faces, 442 edges, 306 vertices).

A message reporting invalid geometry or a shell part (not solid with 1 cell), the user has to repeat the CAD export from *3-matic* using the *CAD Link* tool with refined parameters.

*Importing the **socket** as 3D SHELL geometry* is identical to importing a solid part except for using the option SHELL instead of SOLID (Figure 21)

### **Meshing part** (individual successive operations)

The FEA mesh of a part obtained in *ABAQUS* is more efficient than the one obtained in medical CAD software such as *Mimics*. An external or surface mesh of similar element size in both options, *Mimics* and *ABAQUS*, results in reduced number of

volume mesh when *ABAQUS* adaptive mesh rules by allowing size growth of the interior elements. Consequently, the total number of degrees of freedom of the *Mimics* mesh is many times higher than the corresponding *ABAQUS* mesh. Also obtaining a FEA mesh in *ABAQUS* is used as a verification step for the imported 3D geometries. In other words, successful mesh is obtained for a solid part, e.g. bones, provides further verification of correct imported geometries.

### Mesh module:

Seed part: Figure 23

Assign seed size (this is the element side length in meters, e.g. 0.008 m)

Accept defaults in terms of curvature control and minimum size factor

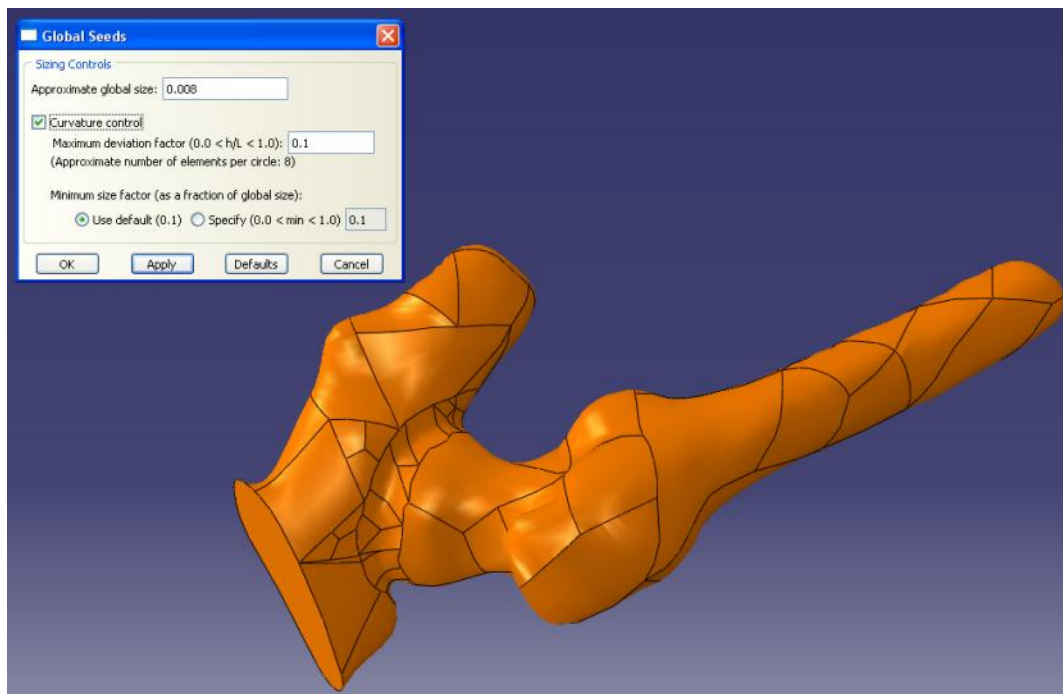


Figure 23: Mesh module, seed part

Mesh Controls: Figure 24

Select **T**etrahedron mesh (since 3D geometry was developed using triangulation)

Accept defaults algorithm with increasing size of interior elements

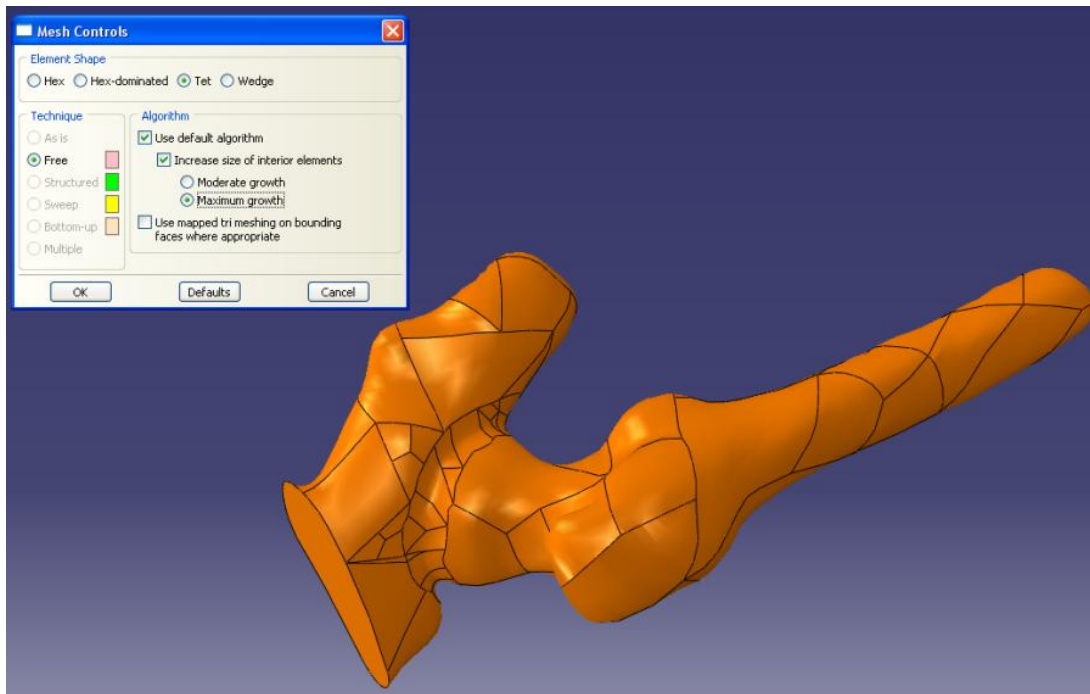


Figure 24: Mesh module, mesh controls

Element Type: Figure 25

*Element library Standard, Geometric Order Linear, Family 3D stress*

*Tet element controls: accept defaults, element is C3D4: 4-node linear tetrahedron*

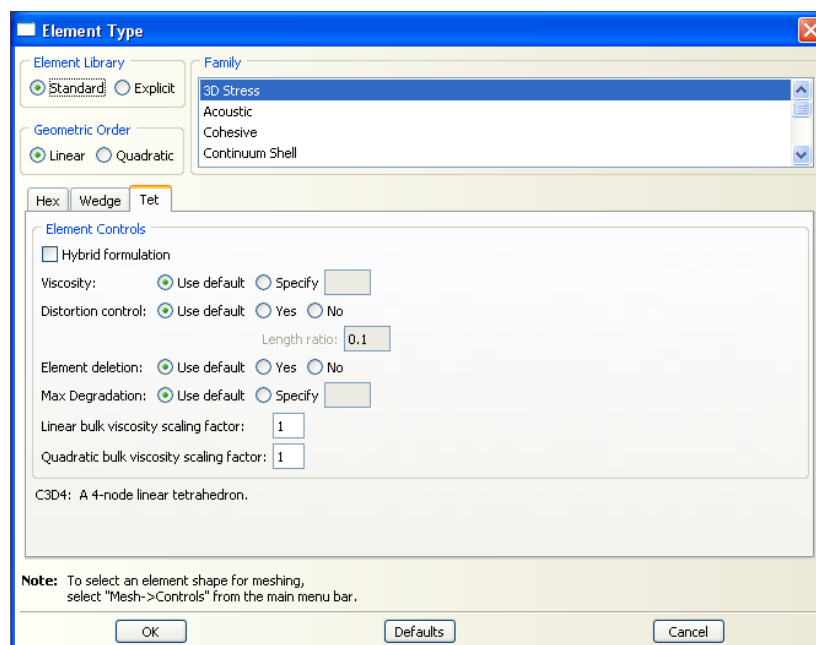


Figure 25: Mesh module, element type



Mesh part: Figure 26

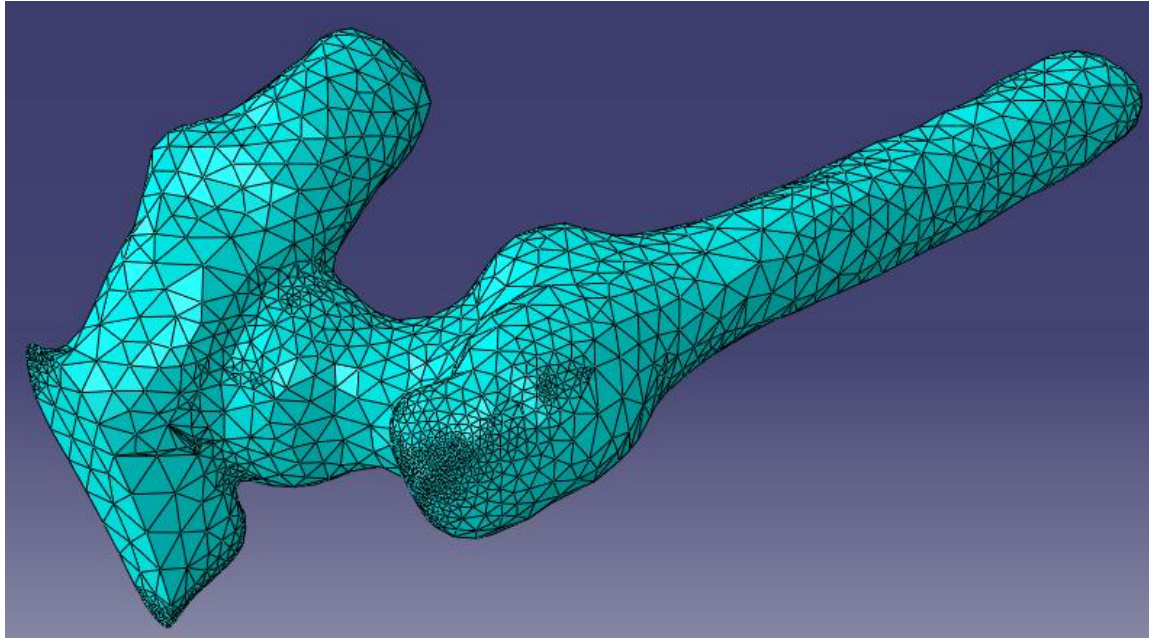


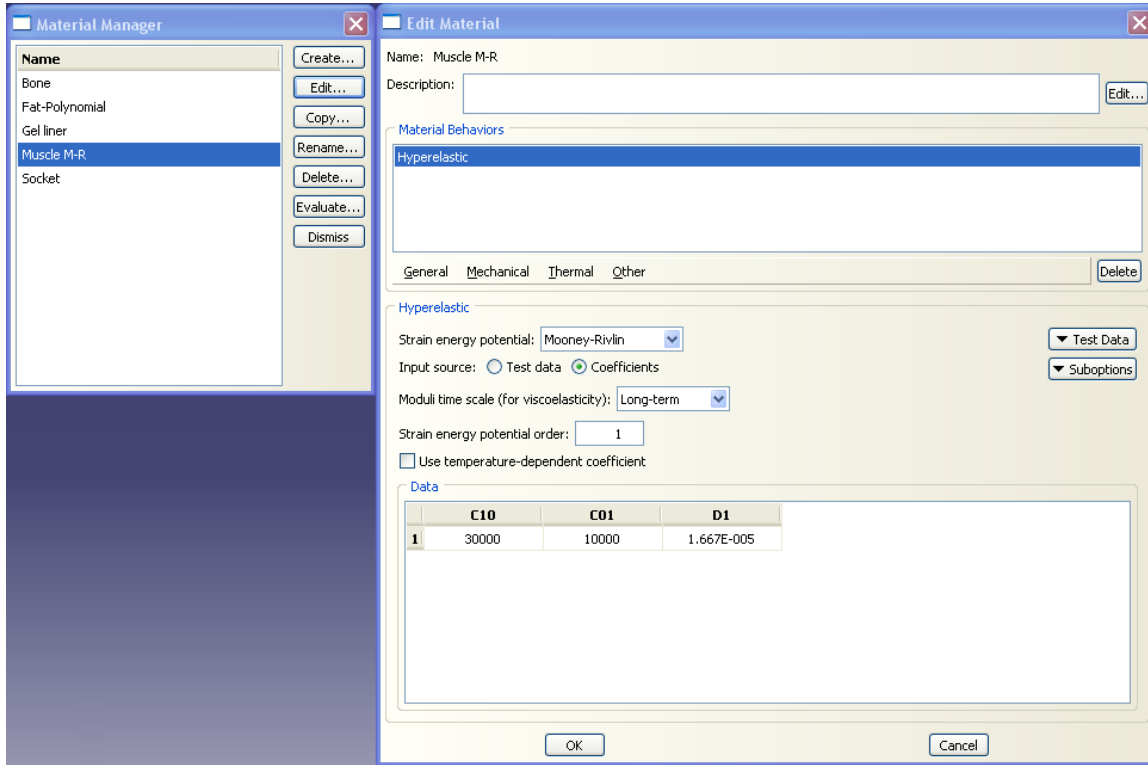
Figure 26: Mesh module, final mesh

### Property Module (Material assignment)

All anatomical entities, bones, muscles and tendons, are assumed to be isotropic and homogeneous. Meanwhile, the material nonlinearities are associated to the rubbery like nature of the soft tissue, i.e. fat and muscle. Hyper-elastic models are used to represent such rubbery behavior in terms of first and second order expressions describing the strain energy function of the muscle and fat tissue, respectively. The Mooney-Rivlin material model assigned to the muscle is expressed in terms of its strain energy  $W$  as

$$W = C_{10}(\bar{I}_1 - 3) + C_{01}(\bar{I}_2 - 3) + \frac{1}{d}(J - 1)^2$$

Where  $\bar{I}_1$  and,  $\bar{I}_2$  are the first and second deviatoric strain invariants and  $J$  is the determinant of the deformation gradient. The strain energy parameters  $C_{10}$ ,  $C_{01}$  and  $d$  take the values,  $C_{10} = 30$  kPa,  $C_{01} = 10$  kPa and  $d = 1.667 \times 10^{-5} \text{ Pa}^{-1}$ . See Figure 27.

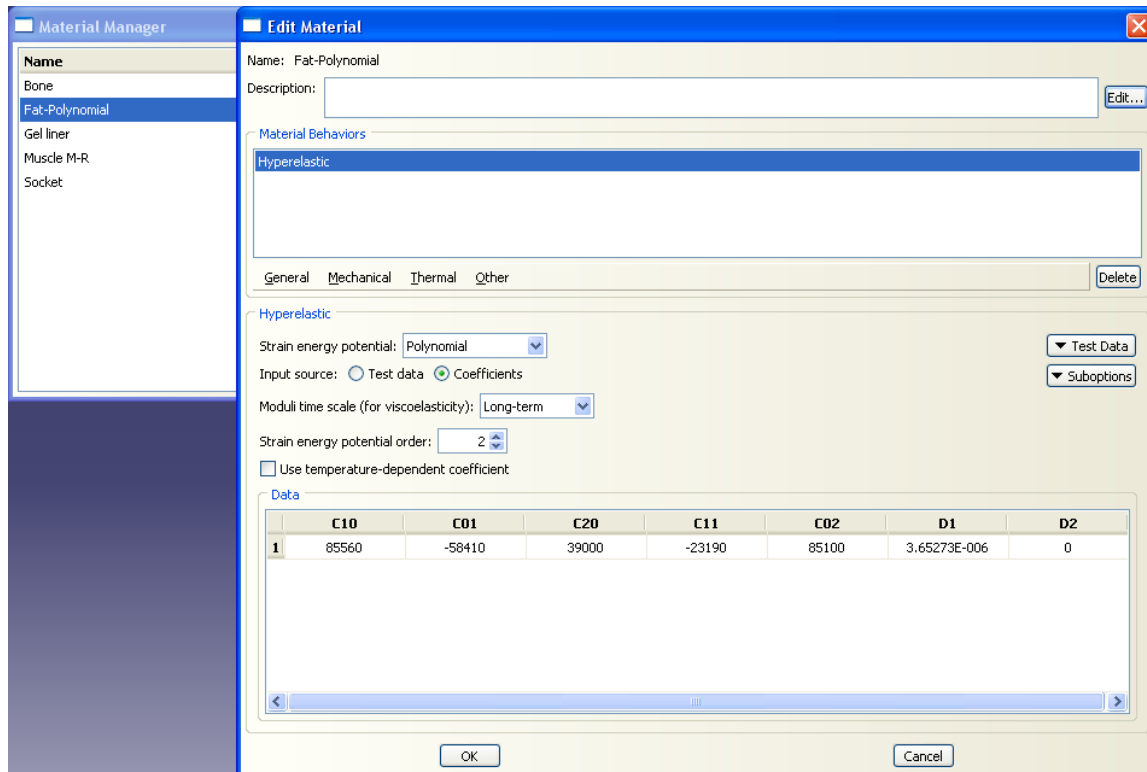


**Figure 27: The Mooney-Rivlin material model assigned to the muscle**

While a second order polynomial strain energy  $W$  utilized to describe the hyper-elastic fat tissue behavior is

$$W = \sum_{i+j=1}^2 C_{ij} (\bar{I}_1 - 3)^i (\bar{I}_2 - 3)^j + \sum_{i=1}^2 \frac{1}{D_i} (J - 1)^{2i}$$

Where  $\bar{I}_1$  and,  $\bar{I}_2$  are the first and second deviatoric strain invariants and  $J$  is the determinant of the deformation gradient. The strain energy parameters assume the values  $C_{10} = 85.56$  kPa,  $C_{01} = -58.41$  kPa,  $C_{20} = 39$  kPa,  $C_{11} = -23.19$  kPa,  $C_{02} = 85.1$  kPa,  $D_1 = 3.653 \times 10^{-6}$  Pa<sup>-1</sup> and  $D_2 = 0.0$  Pa<sup>-1</sup> See Figure 28.



**Figure 28: A second order polynomial strain energy assigned to the fat**

Other anatomical entities or parts such as bones and tendons are assigned linear elastic material models according to literature. Also non-anatomical parts such as the gel liner and the socket are assigned linear elastic material properties. Table 15 provides the linear elastic material properties used in the analysis.

**Table 15: Linear Isotropic material properties**

Material	Young's Modulus (Pa)	Poisson's Ratio	Thermal expansion coefficient ( $^{\circ}\text{C}^{-1}$ )
Bone	$7.3 \times 10^9$	0.3	
Tendon	$2.0 \times 10^8$	0.3	
Gel Liner	$5.17 \times 10^6$	0.3	
Socket (polypropylene)	$1.5 \times 10^9$	0.3	$8.6 \times 10^{-5}$

## Assembly Module

The user creates instances associated to all imported parts. Figure 18 includes all the instances created for the TT case (from left to right, Muscles, Bones, Gel liner, Socket and Fat). Figure 29 is obtained in exploded view, while correct parts import demonstrated identical reference or global coordinates as shown in Figure 30.

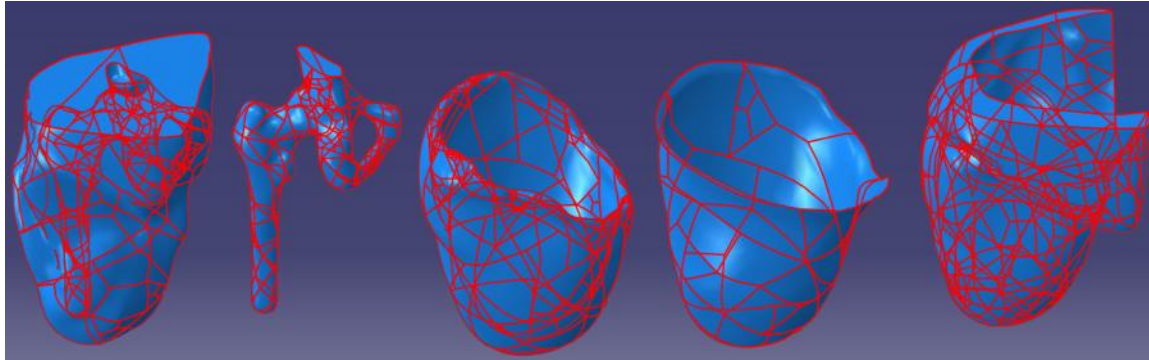


Figure 29: Exploded view of parts import

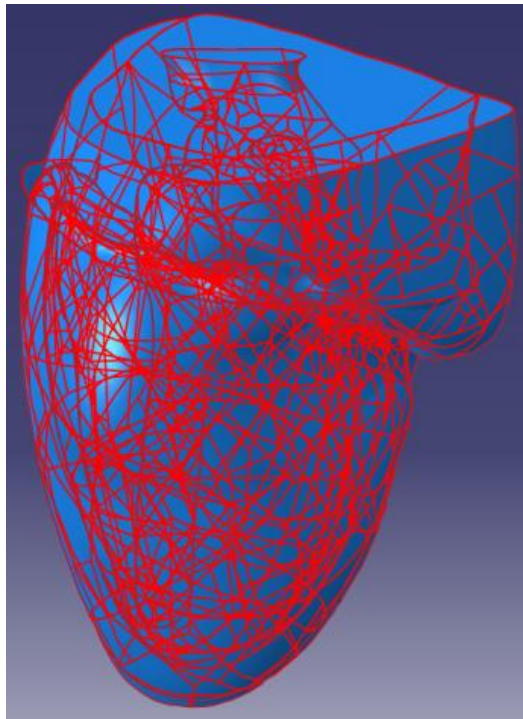


Figure 30: Identical global coordinate system for imported parts

## Step Module

The *model developer* creates a number of analysis steps starting Socket Donning performed followed by a number of load cases associated to standing and motion kinetics. Socket donning as the initial step of analysis represented a challenge in terms of its dynamic nature to simulate sliding the socket up onto the RL. Dynamic analysis in any FEA software is time consuming and of high complexity being associated to many convergence iterations of nonlinear deformation steps and utilizing nonlinear material models.

The socket donning simulation challenge was overcome by replacing the dynamic analysis of sliding the socket up and onto the RL by a thermal shrinking the socket over the RL. In the initial step of the analysis the socket is aligned at the distal end of the RL. Socket donning is performed in two analysis steps, the first step is to thermally expand the socket beyond the external boundaries of the RL while the in the second step the socket undergoes thermal shrinkage to its original dimensions and hence shrinks over the RL.

The standing and walking simulations are simulated each in a separate analysis with a loading applied at the distal end of the socket corresponding to half the body weight, full body weight or the forces and moments associated to phases of gait. Load application method will be introduced in the section dedicated to “Load Module”.

The *model developer* creates all analysis steps as static general steps accepting all defaults except for setting “convert severe discontinuity iteration” set to ON. Figure 31 provides a screen capture of the options in the step module.

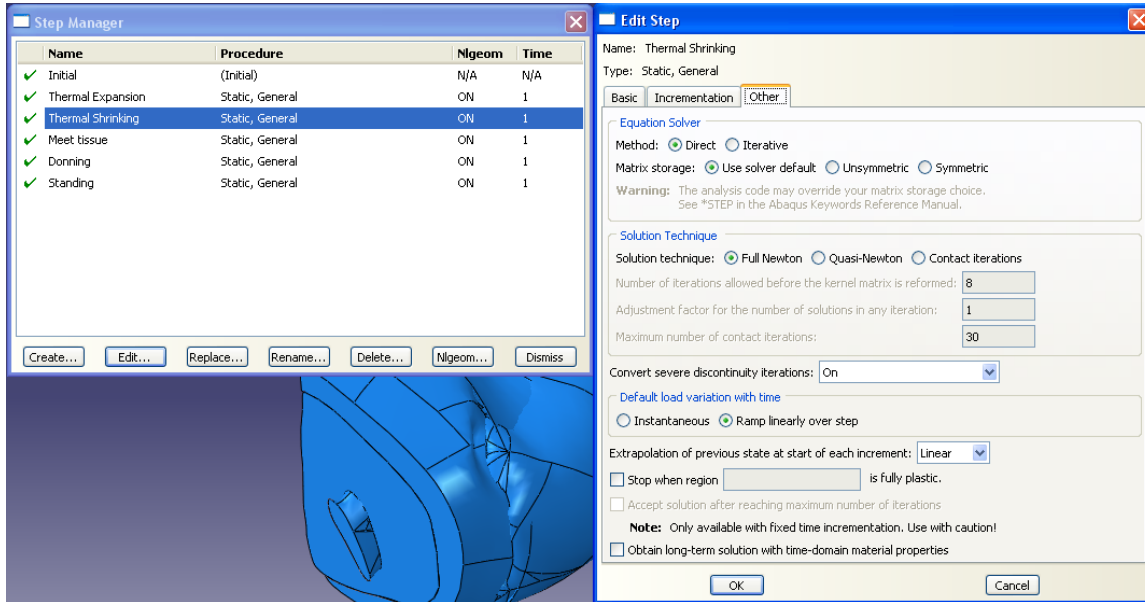


Figure 31: Step Module

## Interaction Module

One of the major advantages of ABAQUS FEA software is its well developed interaction module ranking it superior to all other commercial FEA software. ABAQUS provides contact and constraint detection tool that will detect contact surfaces between any two or more entities (parts) selected by *model developer*. Also ABAQUS has an automated contact subroutine that provides a variety of automated contact properties for realistic normal or tangential surface to surface behavior.

Two major types of contact are used. Among all anatomical entities contact “tie” constraint is established in which matched displacements are enforced along the contact interface. Whereas, the socket/gel liner and socket/tissue contact interaction is identified as hard contact normal behavior (no penetration) and a frictional tangential behavior with coefficient of friction  $\mu = 0.3$ . Figure 32 provides all identified contact surfaces in the TT model as per the extended contact matrix provided in Table III. Figure 33 provides the parameters chosen for the contact interaction.

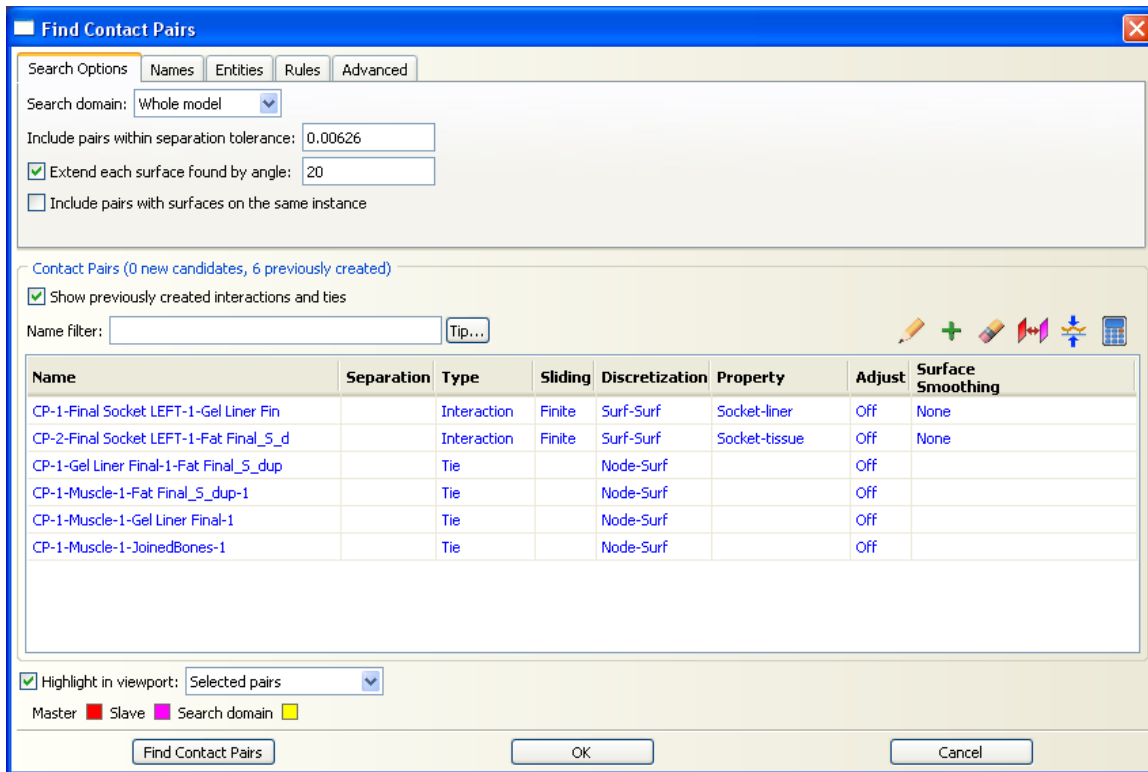


Figure 32: Extended contact matrix applied through ABAQUS detection tool

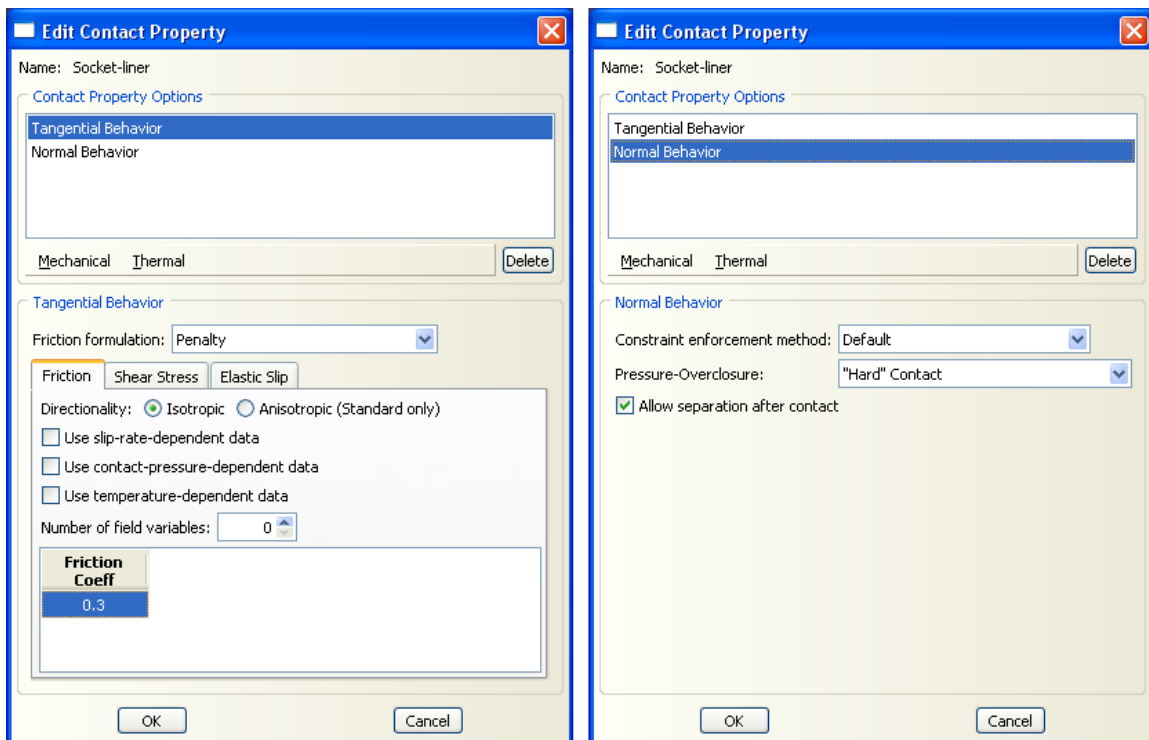
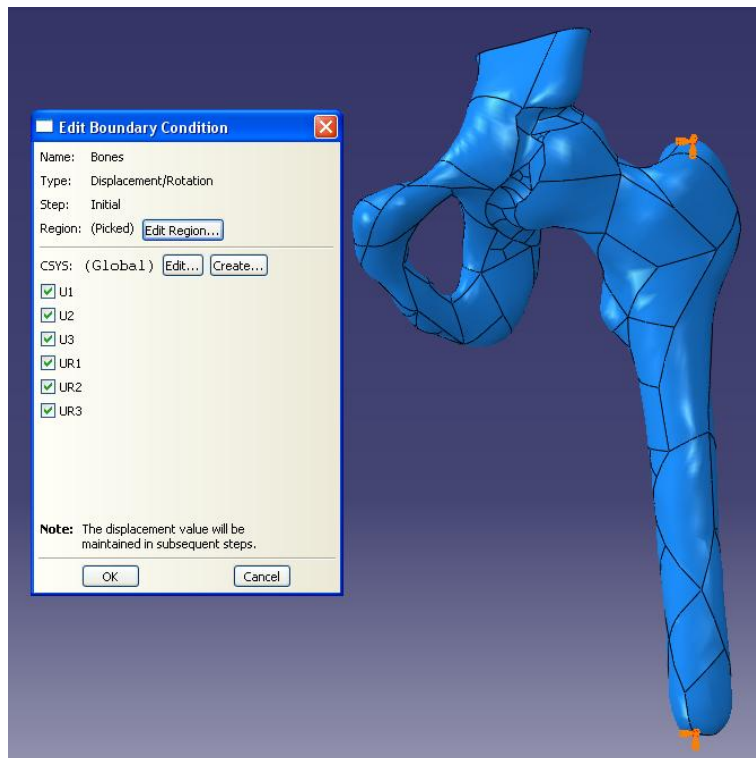


Figure 33: Socket interaction property with the gel liner

## Load Module

In the load module the model developer will identify the Boundary Conditions (BCs), predefined field, and applied loads. In contact problems involving nonlinear geometric deformation identifying the BCs correctly and accurately is essential for analysis completion. If the BCs are not sufficient to prevent rigid body motion/rotation, severe discontinuity iteration arise signifying separation of contact surfaces and preventing the analysis from completion.

*Boundary conditions:* The femur is fixed in space along the top and bottom points as shown in Figure 34. All six degrees of freedom, translation and rotation, are constrained at the top and bottom points of the femur.



**Figure 34: Boundary conditions applied to the RL**

*Predefined field:* a temperature field constant through the thickness is applied to the socket in the expansion step. The predefined field is set to initial or zero value in the socket shrinkage step. During both thermal expansion and shrinkage a distal point on the socket is constrained in all six degrees of freedom. Figure 35 shows a predefined



thermal field of 5000 °C applied to the prosthetic socket in the thermal expansion step and reset to initial in the thermal shrinkage step\

*Loading:* standing example, full body weight is applied vertically to the distal point of the socket (same point was previously constrained during the donning simulation). Figure 36 shows the load application point at the distal end with concentrated force of 800 N (equivalent to the patient’s full weight of 180 lb).

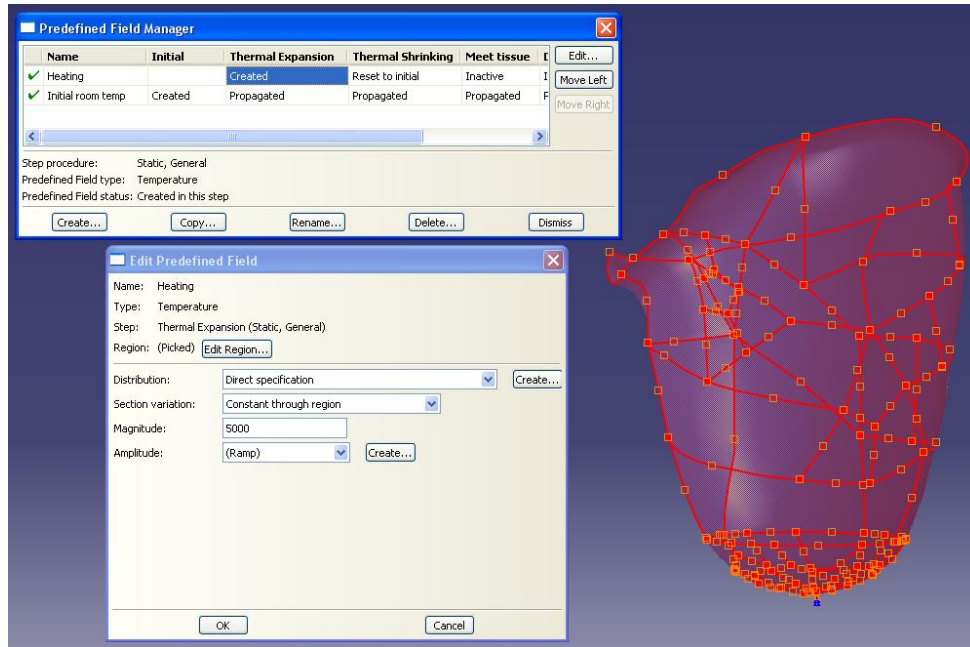


Figure 35: Predefined thermal field

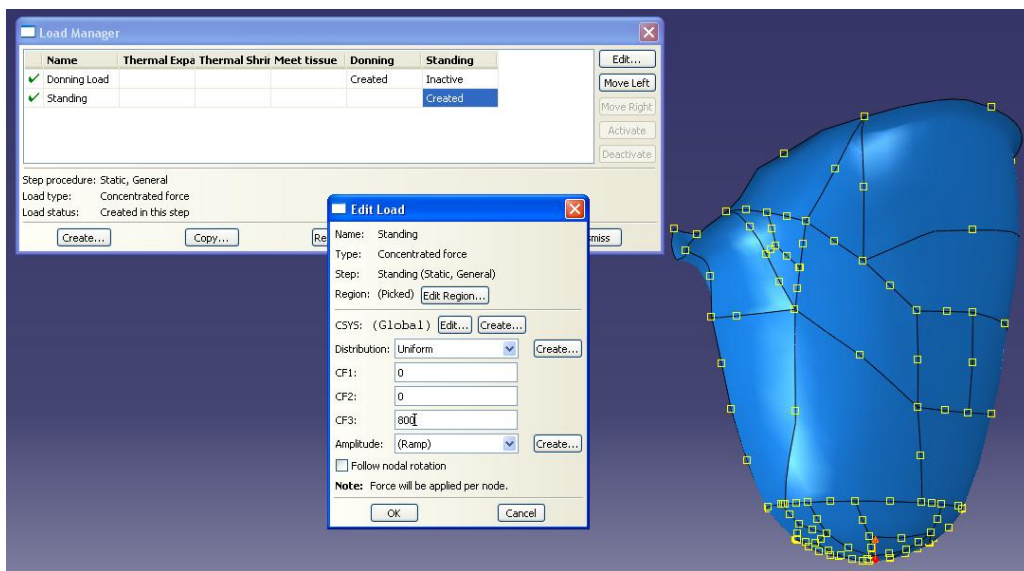


Figure 36: Applied load for standing load case

## **Job Module**

The Job module is used to Data Check or to submit the developed FEA. The module defaults are accepted throughout. The analysis requires parallelization in order to become cost effective. Therefore 8 parallel processors are used to allow the simulation in general run under 30 minutes.

## **FEA Analysis Results**

FEA being conducted according to computational anatomy principals facilitated extracting important information such as the function of gel liner in minimizing the pressure distribution over the RL, stress distribution versus pressure distribution over individual anatomical entities or undeformed versus deformed shape comparison.

### **Analysis results, a transtibial case**

A transtibial case corresponding to TT01 is used to demonstrate the variety of information that can be extracted from the FEA. The FEA model specifics are obtained utilizing a mesh with 112600 C3D4 linear tetrahedrons elements for the anatomy and 1115 elements S4R shell elements for the socket, a total of 28409 Nodes with 114327 Degrees of Freedom. The analysis is performed in 25 minutes including standing or motion kinetics.

### ***The pressure distribution, identifying the major function of the gel liner***

At dual limb support pressure distribution over the gel liner is compared to the pressure distribution over the skin, i.e. on the RL. This comparison shows the function of the gel liner in terms of protecting the RL from excessive pressure. Figures 37 to 40 show pressure distribution comparison in the four different views, namely, anterior, posterior, lateral and medial views.

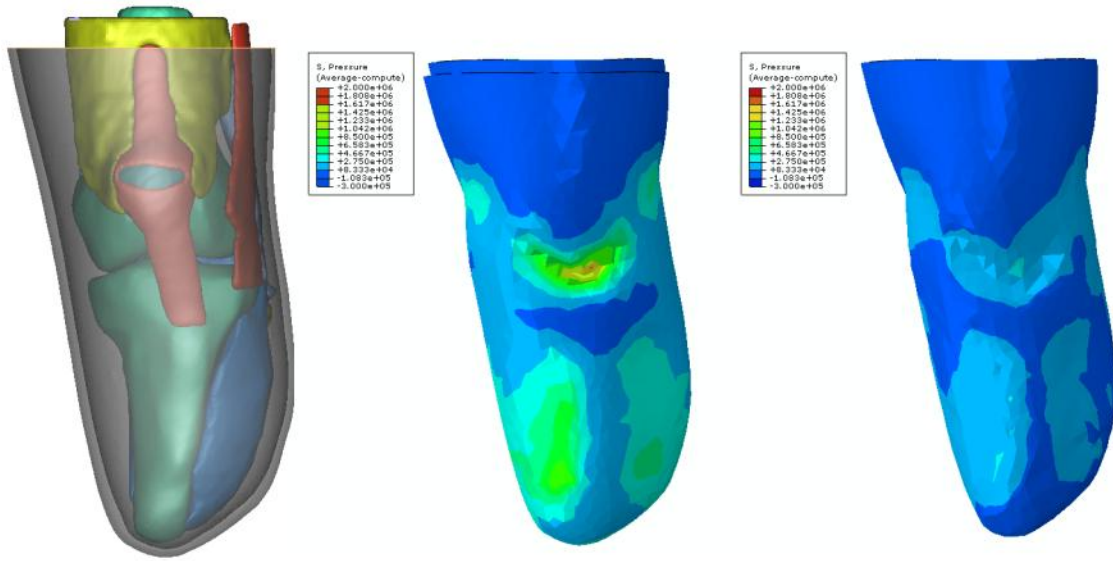


Figure 37: Pressure comparison over gel liner vs. skin – anterior view

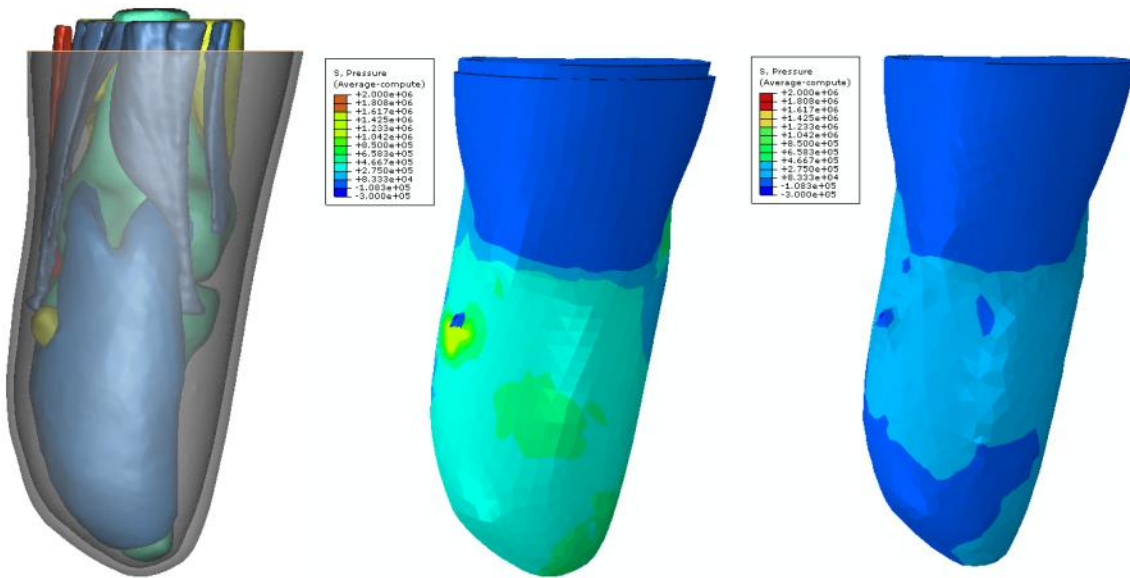


Figure 38: Pressure comparison over gel liner vs. skin – posterior view

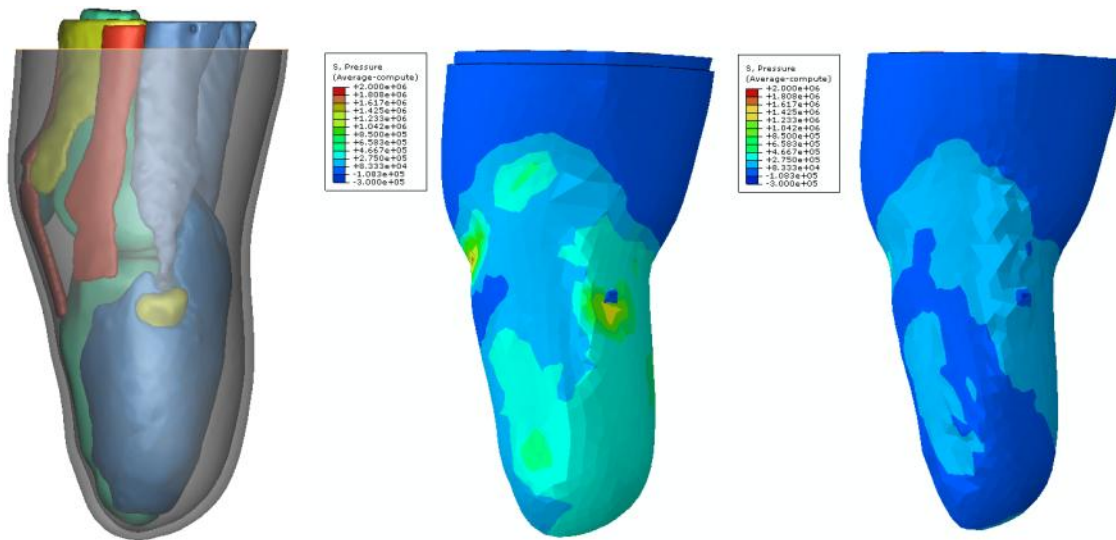


Figure 39: Pressure comparison over gel liner vs. skin – lateral view

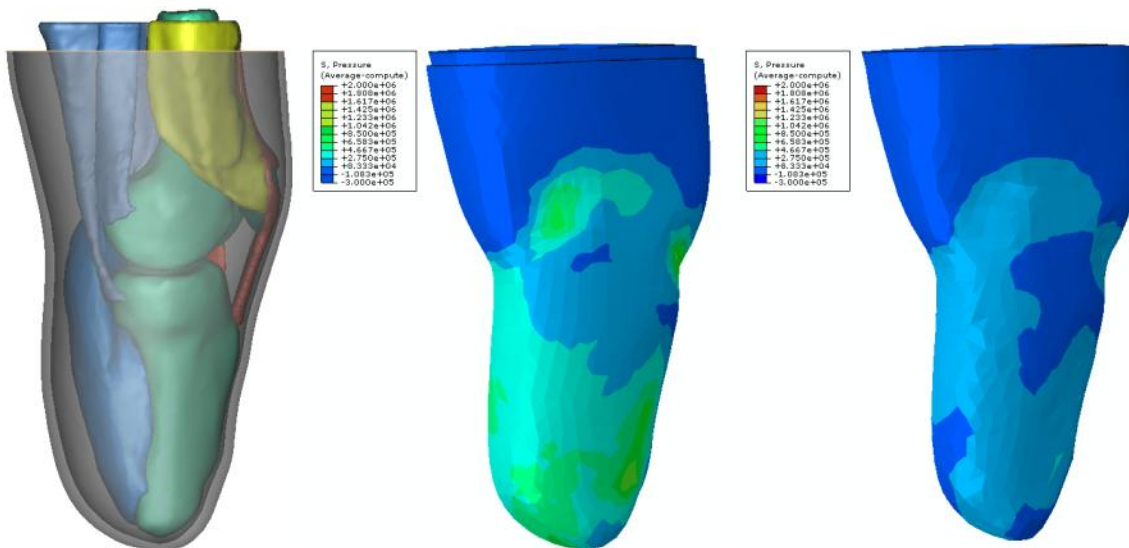


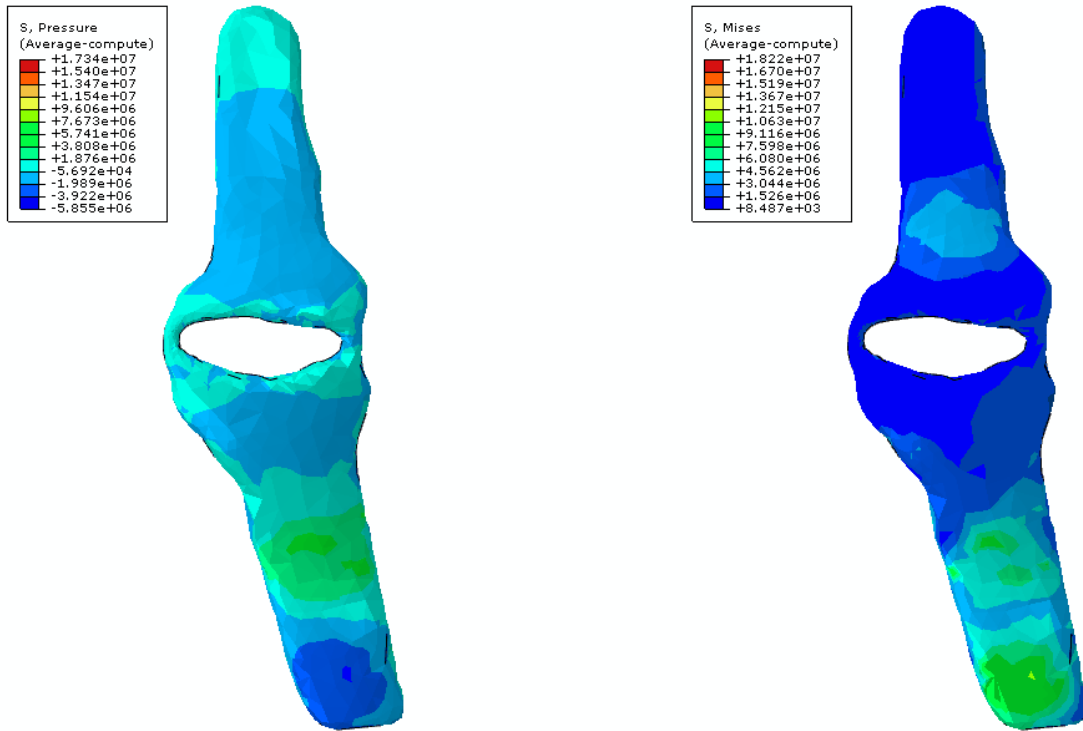
Figure 40: Pressure comparison over gel liner vs. skin – medial view

Also socket rectification efficiency can be seen in, for example, Figure 39 when noticing a pressure relief area around the fibula's head.

### External versus internal load comparison, i.e. pressure versus stress

The patellar tendon/bar is studied by comparing the pressure (external load) versus the stress (internal load) at dual limb support. It can be noticed in Figure 41 that the pressure distribution at the tendon's attachment point to the tibia is very low. Meanwhile, this very low pressure corresponds to a high tensile stresses at the same

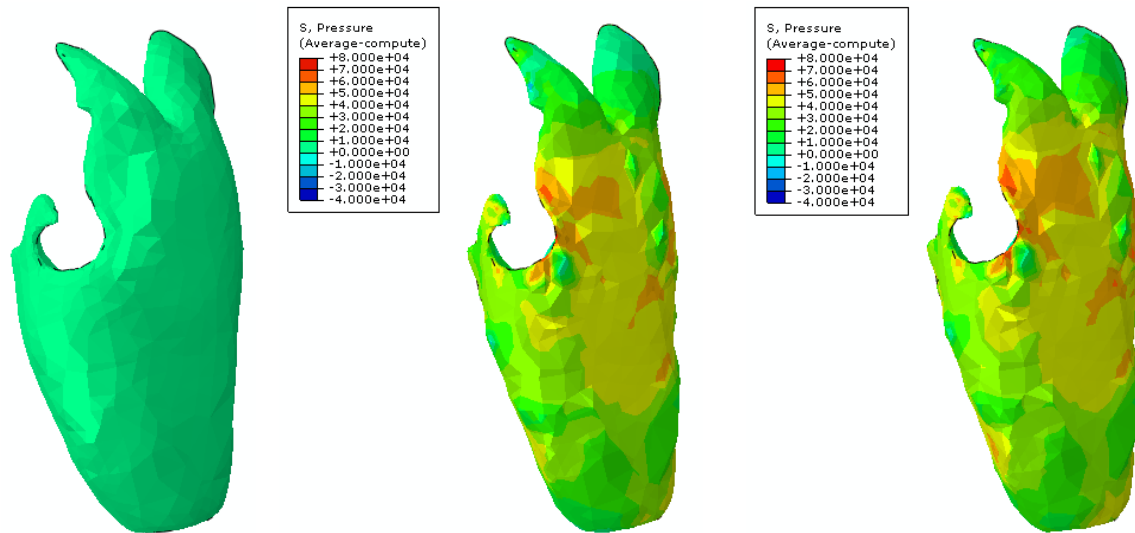
location. Will this tensile stress cause future complication to the patient, will it cause the tendon to adapt to its load requirements.



**Figure 41: External vs. internal loads within the patellar tendon/bar**

*Undeformed vs. deformed shape comparison,*

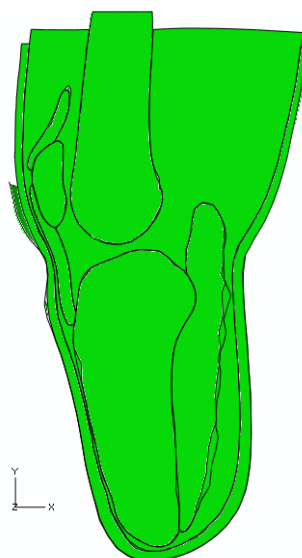
The gastroc shape is compared over stages of analysis, namely, deformed, after socket donning and at dual limb support. The deformed shape of a muscle (when compared in terms of volume reduction) determines the compressibility of the muscle and hence may become an important parameter used to identify muscle atrophy state. Figure 42 provides the undeformed versus deformed shapes of the gastroc together with the pressure distribution in loaded cases.



**Figure 42: Undeformed shape vs. deformed shapes, associated to socket donning and dual limb support**

Multiple data can be extracted from the FEA analysis. Meanwhile for the socket design purpose the pressure distribution over the skin is of specific importance. This pressure distribution should be compared with a reference value corresponding to the threshold of pain in order to optimize the socket shape. An animated simulation (video file) is attached to the manual to visually demonstrate the entire analysis)

A final illustration is depicted in Figure 43 showing a sectional view of the deformed shape in the case of dual limb support.



**Figure 43: Sectional view in the deformed shape at dual limb support**

## Analysis results, a transfemoral case

A transfemoral case represents less challenge in modeling when compared to transtibial cases. Arriving at much simplified anatomy by merging anatomical features of the same family, e.g. all muscles, into one muscle community of simple shape is reason to the inherent simplicity of transfemoral case.

### *The pressure distribution*, identifying the major function of the gel liner

The pressure distribution over the gel liner in this case is about one order of magnitude higher than the corresponding values over the fat tissue (i.e. skin). Figure 44 shows the efficient pressure reduction gained by using the gel liner. The function of the gel liner is well known and documented in literature meanwhile the current FEA present a quantitative tool rather than qualitative assessments of the gel liner. Figure 45 repeats the same results in Figure 44 using a different scale for the pressure distribution in the fat tissue. The pressure limits in this scale is about one order of magnitude less than the ones used for the pressure distribution in the gel liner.

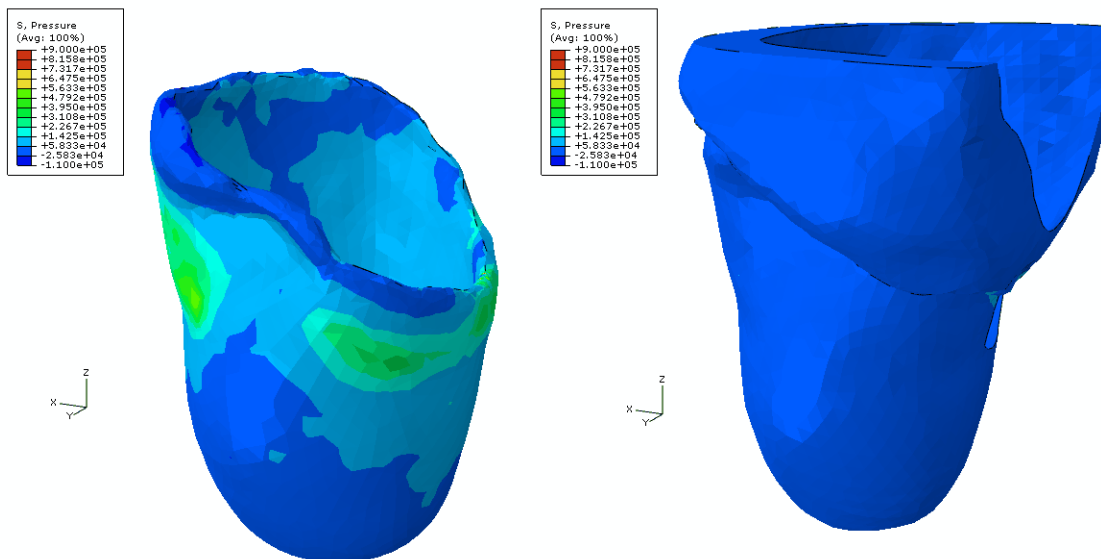


Figure 44: Pressure distribution over gel liner vs. skin – single limb support. Same pressure range or scale.

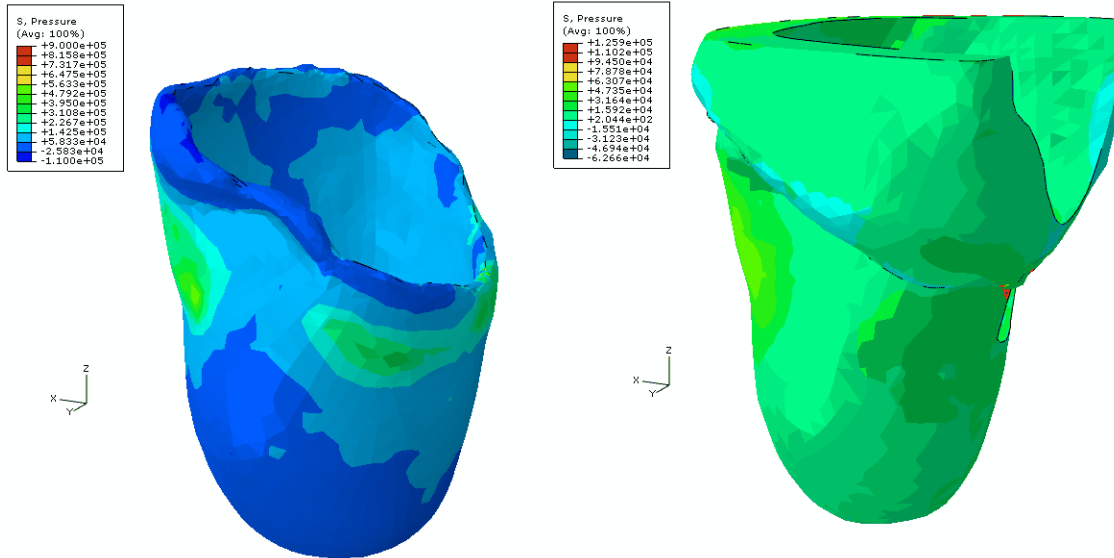


Figure 45: Pressure distribution over gel liner vs. skin – single limb support. Different pressure range or scale

***The stress distribution, in the bones community***

The stress distribution in the bones, Figure 46, shows very low stress distribution in the ischium. Figure 47 provides the stress distribution the bones with the socket in view.

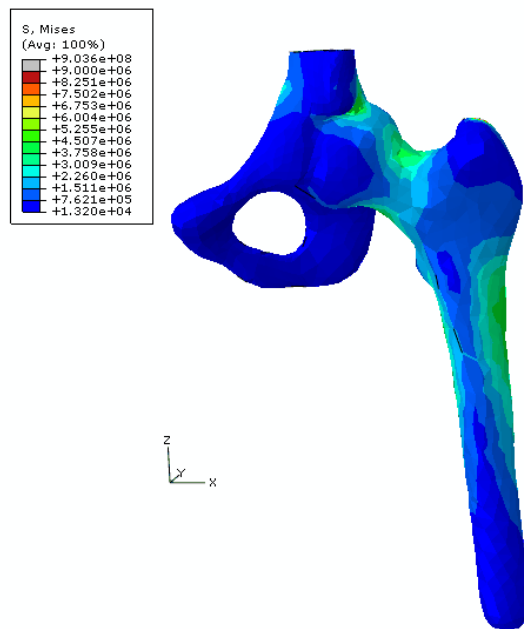
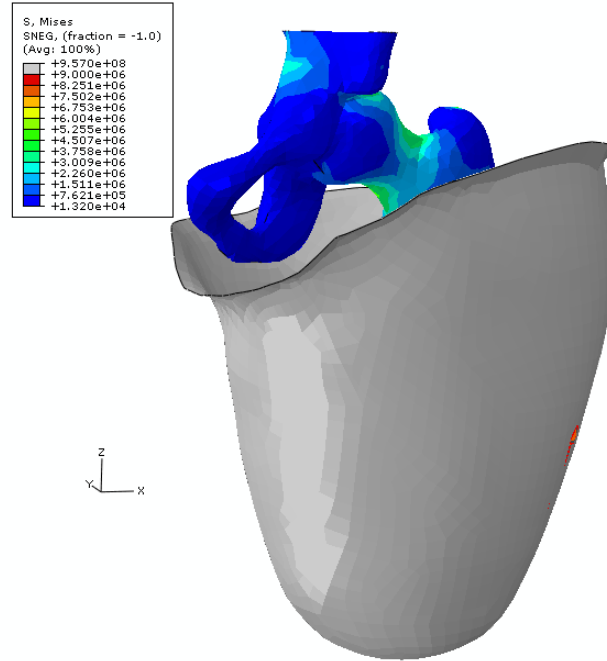


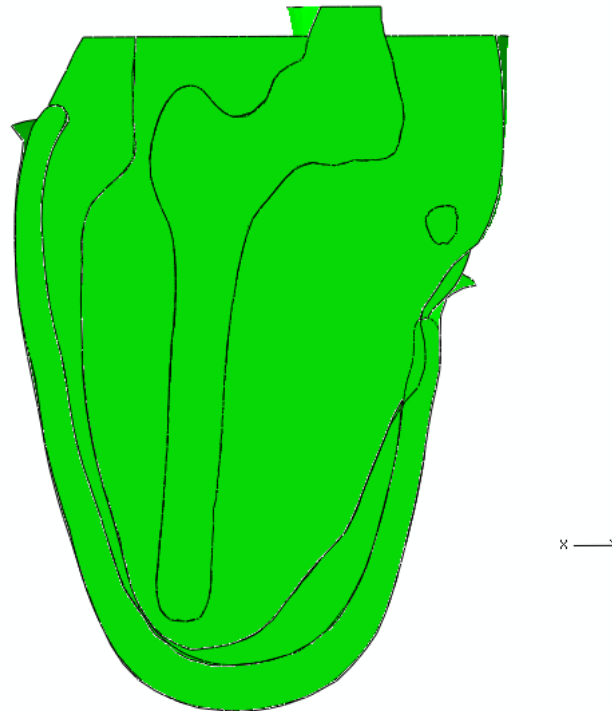
Figure 46: Stress distribution in the ischium





**Figure 47: Stress distribution in the ischium with the socket in view**

A section is performed in the deformed shape for single limb support loading case and shown in Figure 48.



**Figure 48: Sectional view for single limb support**

## FEA Challenges

### Pressure measurements and verification

The pressure distribution over the RL limb is predicted using FEA. This pressure distribution is to be used to optimize the socket shape. Therefore the accuracy of the predicted values is of great importance. Hence verification of the predicted pressure by comparison to measured values is essential. The Zebra sensor system (SensorTech) was suggested as reliable pressure sensor that can conform to irregular geometry and is not associated with any size penalty being introduced as very thin sheets. Meanwhile the software that controls the data sampling process remains under continuous modifications and development to provide the intended versatility of data sampling. Also the sensor measurement system calibration process is still under developed. Therefore the data obtained from the Zebra sensors are not accurate. Consequently these data could not be used for the purpose of verification of the FEA predictions.

The Georgia Tech team MGDPS exhausted a multiple number of iterations in cooperation with SensorTech in order to extract accurate pressure measurements. Meanwhile all these attempts lead to no success. Pressure measurement as a validation step consumed good percentage of the time planned for further development and application of the FEA. Hence a major challenge is to measure the pressure within the socket in order to provide accurate verification of the FEA.



**Figure 49: Sample of one of the Zebra Sensor sockets fabricated for TT01**

### Material models

The current material models used for soft tissue are obtained from open literature and optioned for healthy tissue. Meanwhile the mechanical properties of the soft tissue within the RL are dependent on the amputation history and the level of activity of the patient. FEA method can be used to predict or characterize the material properties of soft tissue combined with simple experiments.

## ***FEA prosthetist***

The FEA technique can be automated to perform the socket fitting trials on a patient to attain better socket fit. Meanwhile, the FEA cannot replace a prosthetist being licensed to work with human subjects as licensing issues will arise.

## **FEA Conclusions**

### **Anatomically correct analysis**

Anatomically correct FEA of prosthetic socket interaction with the RL is proposed and developed. The method proved repeatability and general applicability in the case of transfemoral, transtibial amputation alike. The current FEA allowed utilizing identifiable anatomical entities to construct the RL model. Therefore realistic conclusions were obtained regarding the socket fit in terms of inspecting the pressure/stress at critical sites of the RL. This allows the greatest understanding of sockets fit and rectifications and consequently provides a good foundation for enhancing their design.

Incorporating the history of RL health into the FEA (documenting deterioration or atrophy of muscle) will lower the cost of socket maintenance and also provide an insight for further development in the field. Predictive capabilities of the FEA can be utilized by assigning material models associated to less strength to tissues expected to atrophy and hence a better socket shape change/needs and future predictions.

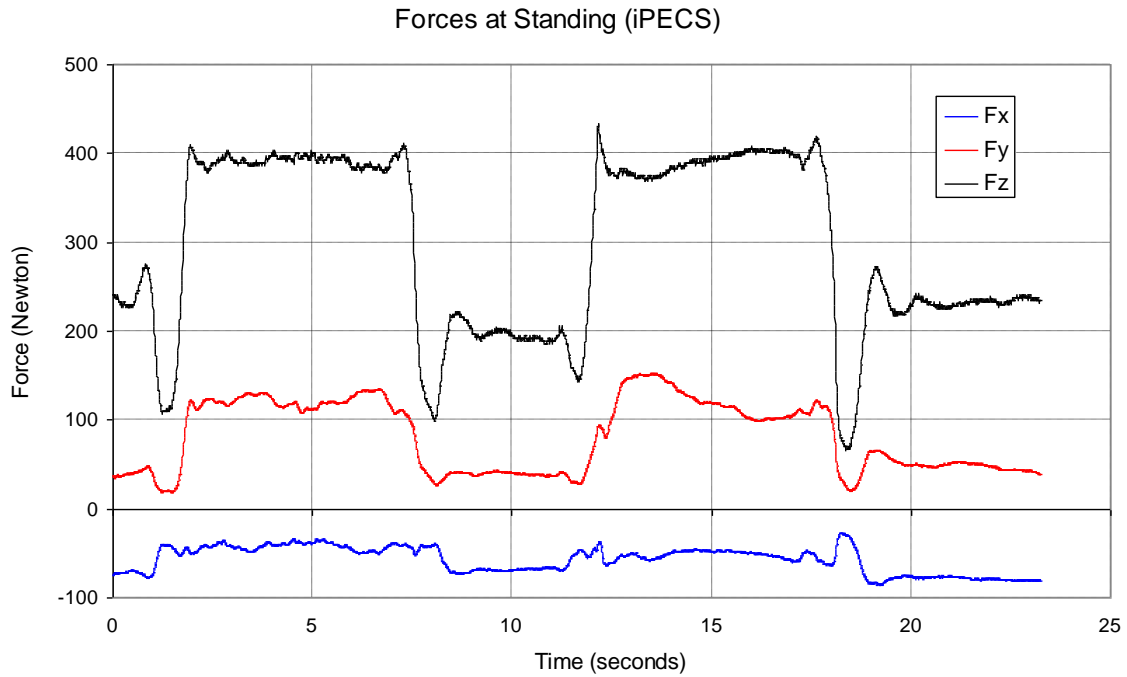
### **Alternative accurate load measurements**

The loading cases of FEA are mainly associated to simulating the socket donning, dual limb support, single limb support (prosthetic side) and walking gait. For the donning simulation there is no significant value for the applied load. While for the standing and walking exercises the iPECS system is used to measure the forces and moments applied to the distal end of the prosthetic socket (See Figures 50 - 52). Simple relationships are used to translate the measured loads to the proximal end of the socket and align the local axes of iPECS measurements with the socket's global system of

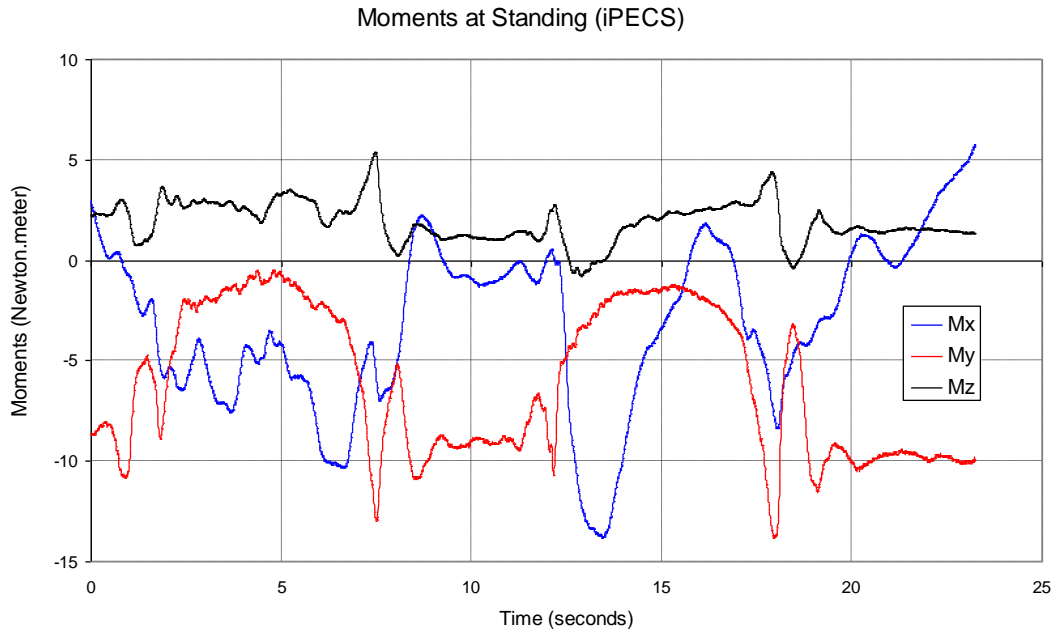


**Figure 50: Subject TT01 on Diagnostic socket instrumented with ZEBRA socket pressure sensors and with an iPECS unit distal to the socket**

axes. A sample data of standing exercise is provided within. In the standing exercise the patient is in dual limb support, and then lifts the sound side to attain single limb support (the prosthetic side). All forces and moments (kinetics data) are collected by the iPECS during this exercise. These loads are transferred at the distal end of the socket to be used in the FEA for standing simulation.



**Figure 51: Standing exercise – force values**



**Figure 52: Standing exercise – moment values**

### **FEA Suggested future work**

The developed FEA methodology represents a first step towards a unified design environment of an adaptive socket. This claim is supported by the used software capabilities and the proven optimal communication. Shape changes of the RL during the course of the day and heat transfer simulations can be performed in *ABAQUS* simulation. Instrumented socket with sensors and actuators can also be modeled in *ABAQUS*. A great advantage is gained by utilizing Mimics Innovation Suite in the current tool by providing the modularity of medical image processing and geometry design and optimization.

## Results and Discussion

This project endeavored to meet the following aims:

1. Develop a model acquisition protocol utilizing a Magnetic Resonance Image (MRI) of a person's residual limb (RL) for the initial model. This included both transfemoral (above the knee) and transtibial (below the knee) amputations.
2. Develop a protocol that would rectify the MRI acquired model by applying tissue density properties to the unique soft tissue structures of that RL so that a computer aided design (CAD) socket can be fabricated for that individual.
3. Test the fit of the CAD socket through instrumented gait analysis (IGA) and RL/socket interface pressure mapping.
4. Utilize the MRI model, CAD socket model and data gathered from the IGA and pressure interface mapping to generate a Finite Element Analysis (FEA) model of a dynamic prosthetic socket.

**Aim #1:** *Develop a model acquisition protocol utilizing a Magnetic Resonance Image (MRI) of a person's residual limb (RL) for the initial model. This included both transfemoral (above the knee) and transtibial (below the knee) amputations.*

This aim was met. The protocol is detailed in the non-deformational shell section and the MRI Scanning sections above.

**Aim #2:** *Develop a protocol that would rectify the MRI acquired model by applying tissue density properties to the unique soft tissue structures of that RL so that a computer aided design (CAD) socket can be fabricated for that individual.*

This aim was partially met. We did investigate and develop a process to rectify the MRI model so that CAD sockets could be fabricated for the subjects at both the transtibial

and transfemoral levels. The process, however, was not tied to unique tissue density properties of the residual limbs. These properties were estimated from the available literature however we were not able to validate these properties in our model without socket pressure measurements.

***Aim #3: Test the fit of the CAD socket through instrumented gait analysis (IGA) and RL/socket interface pressure mapping.***

This aim was partially met. The sockets that were fabricated for TT01 Subject were tested through instrumented gait analysis as well as force/moment analysis through the use of the IPECs component by College Park. We attempted to quantify the RL/socket interface through multiple iterations of sockets and Zebra sensor systems however this critical component was not successful. We did not have additional subjects ambulate in the gait lab.

***Aim #4: Utilize the MRI model, CAD socket model and data gathered from the IGA and pressure interface mapping to generate a Finite Element Analysis (FEA) model of a dynamic prosthetic socket.***

This aim was met. Finite element analysis was performed on the modified sockets generated from the processes above. A novel solution to virtual socket donning was established using thermal expansion to shrink the virtual socket onto the residual limb rather than push the socket up onto the limb as is done in reality.

## Benefits Analysis (including final metrics tables)

The benefits from this project at its conclusion are the establishment of processes that will be beneficial to utilizing this approach to fabricating prosthetic sockets once the expressed limitations are overcome. The specific beneficial processes developed through this project include:

- **Process 1:** Fabrication of a non-deformational shell for either transfemoral or transtibial residual limbs utilized to simulate the residual limb anatomy.
- **Process 2:** MRI Scanning protocols. Through the collaboration with Dr. Terk at Emory and the research team at Georgia Tech, protocols for positioning as well as for scanning were established for both transtibial and transfemoral subjects.
- **Process 3:** Transferring MRI DICOM files and Segmentation of the residual limb tissue components and liner could be performed.
- **Process 4:** The residual limb modeling process was established and refined through the six socket iterations.
- **Process 5:** CAD Socket rectification. This process was established taking the STL files from 3 Matic and transferring them to CANFIT for rectification. Once rectified, the socket was converted back to a STL file with the orientation maintained thereby allowing comparison of the socket to the underlying anatomy in 3-Matic as well as to facilitate the finite element analysis in ABAQUS.
- **Process 6:** Refining the residual limb anatomical structures in preparation for finite element analysis.
- **Process 7:** Finite element analysis of donning a socket onto a residual limb as well as loading the residual limb in single and double limb standing.

## Implementation Status

In order for this project to transition to a clinical feasible platform, a number of limitations will need to be overcome. First of all, the outcome from this process must be significantly better than the existing “sockets by experience” methods being utilized today as the costs will be greater. Outcomes that would justify the increased cost would be:



- The ability to predict the sockets a wearer will need over time as the process of edema reduction and residual limb atrophy is quantifiable. In theory, one scan could be completed and the sockets the wearer will need over the next 6 months to a year could be fabricated and ready for them in advance.
- The ability to custom fabricate sockets that are optimized for pressure distribution thereby creating an “ideal” socket for that wearer.
- The ability to optimize the socket configuration so that instead of a static socket, a dynamic, multi property socket could be road mapped through FEA and then fabricated through advanced socket fabrication techniques.

The greatest limitation to the projects’ implementation was a method to obtain accurate and reliable socket pressure information. Multiple iterations of the Zebra Socket system by SensorTech were applied but in the end the results were not reliable. Without pressure data, the FEA assumptions cannot be validated and hence, there is no means to optimize the socket fitting process in the virtual world.

Other limitations to implementation include tissue segmentation from the MRI scans. This process needs to be automated. While Materialise was quite responsive to the feedback we provided them and they released multiple versions during the course of the project, the segmentation still leaves much to be desired. The time required to complete the segmentation process is highly dependent upon the experience of the person performing the segmentation process.

Once the segmentation is complete, the prosthetists’ input is required in order to rectify the residual limb socket model. Here again, the experience of the prosthetist plays a role in the rectification process. Ideally this process could be driven automatically depending on the quantity and quality of the underlying soft tissues but at this time, the rectifications must be done manually in order to have a jumping off point. Once we have enough data from residual limb/socket interfacing through finite element analysis, an algorithm could be created to automatically rectify residual limb models. Given that we do not yet have a means to obtain pressure information in order to validate the finite element analysis, we are still a ways off from automatic socket rectifications based on a segmented residual limb from and MRI scan alone.

In Summary, while this project was not able to meet all of its ambitious aims, it did make significant progress in developing processes towards meeting these aims. Automated prosthetic socket fabrication from MRI scanning is possible at this time, however not necessarily cost effective. As the software continues to improve and the costs associated with scanning decline, it is conceivable that MRI scanning will be not only feasible but will eliminate much of the guess work from prosthetic socket fabrication.

This project demonstrated that it is possible to utilize Finite Element Analysis for prosthetic socket fit assessment. We were not able to take the analysis to its full capacity for lack of accurate and reliable socket pressure measurements. Technology in this realm also continues to improve and it is likely that the ability to identify socket pressures in real time will be a reality in the next few years.

Given the progress made on this project, it will be feasible for prosthetic socket fabrication and optimization to be made from MRI scans in the near future. Critical steps towards this reality have been made as a result of this Medical Image Generated Dynamic Prosthetic Socket project.

## References

1. Zhang, M., A.F. Mak, and V.C. Roberts, *Finite element modelling of a residual lower-limb in a prosthetic socket: a survey of the development in the first decade*. Medical Engineering & Physics, 1998. **20**(5): p. 360-373.
2. Zheng, Y.P., A.F. Mak, and A.K. Leung, *State-of-the-art methods for geometric and biomechanical assessments of residual limbs: a review*. Journal Of Rehabilitation Research And Development, 2001. **38**(5): p. 487-504.
3. Portnoy, S., et al., *Real-time patient-specific finite element analysis of internal stresses in the soft tissues of a residual limb: a new tool for prosthetic fitting*. Annals Of Biomedical Engineering, 2007. **35**(1): p. 120-135.
4. Douglas, T.S., et al., *Automatic segmentation of magnetic resonance images of the trans-femoral residual limb*. Medical Engineering & Physics, 1998. **20**(10): p. 756-763.
5. Buis, A.W.P., et al., *Magnetic resonance imaging technology in transtibial socket research: a pilot study*. Journal Of Rehabilitation Research And Development, 2006. **43**(7): p. 883-890.
6. Smith, K.E., et al., *Validation of spiral CT and optical surface scanning for lower limb stump volumetry*. Prosthetics and Orthotics International, 1995. **19**(2): p. 97-107.
7. Zachariah, S.G., J.E. Sanders, and G.M. Turkiyyah, *Automated hexahedral mesh generation from biomedical image data: applications in limb prosthetics*. Rehabilitation Engineering, IEEE Transactions on, 1996. **4**(2): p. 91-102.
8. Shuxian, Z., Z. Wanhua, and L. Bingheng, *3D reconstruction of the structure of a residual limb for customising the design of a prosthetic socket*. Medical Engineering & Physics, 2005. **27**(1): p. 67-74.
9. Peery, J.T., et al., *A Three-Dimensional Finite Element Model of the Transibial Residual Limb and Prosthetic Socket to Predict Skin Temperatures*. Neural Systems and Rehabilitation Engineering, IEEE Transactions on, 2006. **14**(3): p. 336-343.
10. Douglas, T., et al., *Ultrasound imaging in lower limb prosthetics*. Neural Systems and Rehabilitation Engineering, IEEE Transactions on, 2002. **10**(1): p. 11-21.
11. Lee, W.C.C., et al., *Finite element modeling of the contact interface between trans-tibial residual limb and prosthetic socket*. Medical Engineering & Physics, 2004. **26**(8): p. 655-662.
12. *MIMICS Accuracy*. [cited 2009 October]; Available from: [www.materialise.com](http://www.materialise.com).
13. Jamali, A.A., et al., *Linear and angular measurements of computer-generated models: Are they accurate, valid, and reliable?* Computer Aided Surgery, 2007. **12**(5): p. 278-285.
14. Gelaude, F., J.V. Sloten, and B. Lauwers, *Accuracy assessment of CT-based outer surface femur meshes*. Computer Aided Surgery, 2008. **13**(4): p. 188-199.
15. Radcliffe C.W., F.J., *The patellar-Tendon Bearing Below Knee Prosthesis*. 1961: University of California Biomechanics Laboratory.